The Effect of Catalyst Layer Cracks on the Mechanical Fatigue of Membrane Electrode Assemblies

Michael Thomas Pestrak

Thesis submitted to the faculty of the Virginia Polytechnic Institute and State University in partial fulfillment of the requirements for the degree of

Master of Science
In
Macromolecular Science and Engineering

Scott W. Case – Committee Chairman
David A. Dillard
Michael W. Ellis

Oct. 8, 2010
Blacksburg, VA 24061

Keywords: Mechanical behavior, fatigue lifetimes, blister test, proton exchange membranes, membrane electrode assembly

The Effect of Catalyst Layer Cracks on the Mechanical Fatigue of Membrane Electrode Assemblies

Michael Thomas Pestrak

ABSTRACT

Mechanical fatigue testing has shown that MEAs (membrane electrode assemblies) fail at lower stresses than PEMs (proton exchange membranes) at comparable times under load. The failure of MEAs at lower stresses is influenced by the presence of mud cracks in the catalyst layers acting as stress concentrators. Fatigue testing of MEAs has shown that smaller-scale cracking occurs in the membrane within these mud cracks, leading to leaking during mechanical fatigue testing and the failure of the membrane. In addition, this testing of MEAs has further established that the cyclic pressurization pattern, which affects the viscoelastic behavior of the membranes, has a significant effect on the relative lifetime of the MEA. To investigate this behavior, pressure-loaded blister tests were performed at 90 °C to determine the biaxial fatigue strength of Gore-Primea® Series 57 MEAs. In these volume-controlled tests, the leak rate was measured as a function of fatigue cycles. Failure was defined as occurring when the leak rate exceeded a specified threshold. Post-mortem characterization FESEM (field emission scanning electron microscopy) was conducted to provide visual documentation of leaking failure sites. To elucidate the viscoelastic behavior of the MEA based on these results, testing was conducted using a DMA to determine the stress relaxation behavior of the membrane. This data was then used in a FEA program (ABAQUS) to determine its effect on the mechanical behavior of the MEAs. A linear damage accumulation model used the ABAQUS results to predict lifetimes of the membrane in the MEAs. The models showed that under volume-controlled loading, the stress decays with time and the stress dropped towards the edges of the blisters. The lifetimes of the MEAs varied depending on the cycling pattern applied. This is important for understanding failure mechanisms of MEAs under fatigue loading, and will help the fuel cell industry in designing membranes that better withstand imposed hygrothermal stresses experienced during typical operating conditions.

Acknowledgements

The author would like to give special thanks to Stephen McCartney and John McIntosh from the Nanoscale Characterization and Fabrication Laboratory (NCFL) at Virginia Tech for their help in generating the FESEM images. I greatly appreciate the help from Mac McCord at Virginia Tech for his help in the design and construction of the bubble point testing fixture. I would also like to thank Mr. Daniel Miller of GM fuel cell Research Labs at Honeoye Falls for the design and construction of the mechanical fatigue blister fixture and the GM fuel cell research group for supplying the Gore-Primea® Series 57 MEA sheets. I want to thank my advisor Dr. Scott Case for his help and advice on the direction of my research. I also greatly appreciate the suggestions given to me concerning my research from my other committee members Dr. David Dillard and Dr. Michael Ellis. I wish to give special thanks to Dr. Yongqiang Li, Dr. Yeh-Hung Lai and Dr. Craig Gittleman from the GM fuel cell research group for their assistance and input on this research project. The author is grateful for the financial support of GM fuel cell Research Labs and to the NSF-IGERT program.

Table of Contents

List of Figures

List of Tables

Chapter 1: Introduction

Fuel cells are one of the most promising alternative energy conversion devices. In particular, they are widely being investigated as an alternative to the internal combustion engine. While the internal combustion engine is fairly efficient and relatively inexpensive to run, it is also a significant source of the greenhouse gas, CO_2, and its cost to run is mostly determined by the price of gasoline, which is forecast to increase due to the rising demand and diminishing reservoirs of crude oil. Fuel cells using hydrogen as the fuel produce nothing but water vapor as the exhaust thus eliminating CO_2 production as long as the hydrogen is generated through carbon-neutral methods. Fuels cells operate by the production of ions and their subsequent transport which results in an electric current which can be utilized to run a device in an external circuit.

One of the most widely researched fuel cells is the proton exchange membrane fuel cell (PEMFC). The PEMFC operates by splitting hydrogen gas into protons and electrons at the anode of the fuel cell. The protons are subsequently transported across a membrane (the proton exchange membrane, or PEM) to the other side of the membrane and combine with oxygen gas and free electrons, thus forming water. The electrons travel through an external circuit from the anode to the cathode, providing the energy needed to run devices such as automobiles. A single fuel cell consists of a central, thin proton-permeable membrane surrounded by catalyst layers, gas diffusion media and bipolar plates. Many individual cells are stacked together to form an actual fuel cell stack. The number of cells depends on power requirements and the amount of space the stacked cells take up. The fuel cell membrane is one of the most critical elements in the fuel cell since it is responsible for the transport of protons and not electrons which are

forced into an external circuit. The catalyst layers are part of the external circuit responsible for the transport of electrons from the anode to the cathode. The catalyst layers also contribute to the hydrogen-oxygen reaction (which is the rate-limiting reaction). The combination of the catalyst layers and the proton exchange membrane (PEM) is called the membrane electrode assembly (MEA).

One of the major obstacles to the commercialization of fuel cells is the operation lifetime of fuel cells. A target of at least 5000 hours of lifetime has been set in order for fuel cells to be able to compete with the internal combustion engine [1]. Currently many of these fuel cells do not yet meet the 5000 hour requirement for commercial use [1]. A potentially major factor in the short lifetimes of fuel cell membranes is the creation of stress concentrations or localized stresses. These stress concentrations can result from several sources including thinning of the membrane in spots due to areas of greater compression within the membrane from the rough surfaces of the gas diffusion layers and the channel design of the bipolar plates. Another potential source for localized stresses is the presence of branching cracks called "mud cracks" in the catalyst layers. These mud cracks are present in the as-received MEA due to the manufacturing process. During manufacturing the catalyst layers are hot-pressed onto the membranes and then allowed to cool and dry which results in either the shrinking of the catalyst layers or the evaporation and loss of chemicals used in the processing of the catalyst materials. The combination of mud cracks with the localized thinning of membranes could lead to accelerated stress concentrations and much shorter lifetimes for the membrane. Thus, the purpose of the current research is the investigation of these mud cracks and their effect on the mechanical behavior or durability of fuel cell membranes.

Background Literature

The two main problems associated with the commercialization of fuel cells are cost and durability [1]. Both of these issues are interrelated since increasing durability often results in rising cots [2]. However, fuel cell commercialization is still valuable due to its potential to reduce air pollution, greenhouse gas emissions and economic dependence on petroleum [2]. Reducing the United States' dependence on foreign oil would be a boon for the US economy. Global warming is one of the most troubling problems humanity will face in the future and reducing greenhouse gas emissions would help in keeping it from going out of control. Thus, there is significant backing behind the commercialization of fuel cell technology.

One of the main avenues for fuel cell technology utilization is the automobile. Currently, the main focus for fuel cells in automotives is the proton exchange membrane fuel cell, or PEMFC [2]. The proton exchange membrane (PEM) was introduced by GE between 1959 and 1964 [3]. Nafion, a particular type of PEM used as the standard fuel cell membrane in vehicles to which many other membranes are compared, was introduced by DuPont in 1966 [3-5]. Nafion belongs to the polyperfluorosulfonic acid group of PEMs [5]. The other main groups of membranes are PEMs containing styrene and derivatives, poly(arylene ether)s, PEMs based on poly(imide)s, high performance polymeric backbones for use in PEMs, polyphosphazene PEMs and other proton conducting moieties, alternative to sulfonation [5]. Specific fuel cell membranes being researched include BPSH, poly(arylene ether sulfone), PATS, poly(arylene thioether sulfone), and sPI, sulfonated polyimide [4, 6, 7]. The chemical structures of these fuel cell membranes are shown in Fig. 1 [4]. BPSH is a particular interesting material since it

could be used at high temperatures (> 100 °C) and can be synthesized in a multiblock copolymer form which allows one to control its morphology and subsequently its performance [6, 7]. Gore-Select is a reinforced Nafion membrane introduced by W. L Gore & Associates in 1999 [3, 8]. The reinforcement layer in Gore-Select has been shown to help with durability [3, 9]. These alternative PEM materials could provide advantages in system performance, cost and operational flexibility [4].

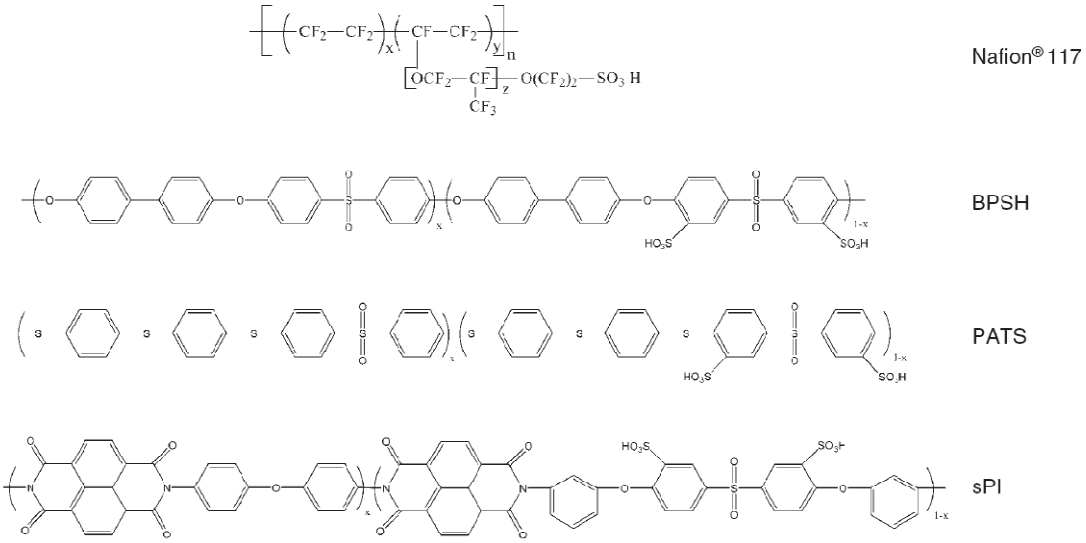

Figure 1: Chemical structures of common fuel cell membranes. Reprinted with permission from [4]. Copyright Wiley-VCH Verlag GmbH & Co. KGaA.

Critical features for polymer electrolytes in fuel cells are high proton conductivity, low permeability to reactants, low electronic conductivity, chemical stability and good mechanical properties [4]. These critical features along with water transport are strongly dependent on polymer chemistry and structure [4]. The four key tunable parameters of fuel cell membranes are the backbone, acid group, ion exchange capacity and processing or history characteristics [4]. The backbone affects the stability and hydrophobic characteristics of the membrane [4]. The acid groups affect the water transport properties and hydrophilic characteristics of the membrane [4]. The ion

exchange capacity, influenced by the acid groups and phase segregation between the backbone and acid groups, influences the performance of the membrane [4]. The processing / history of the membrane have a great influence on the performance and lifetimes of the membranes [4, 10]. Modifying these characteristics through altering the chemical structure of the fuel cell membranes can result in the ideal fuel cell membrane for high performance fuel cells.

In order to achieve commercial success in the automotive sector, a PEMFC must be able to compete with the internal combustion engine. The current status of PEMFC is an operating temperature of ≤ 80 °C, cyclical durability at this temperature of about 2000 hours, H_2 / O_2 crossover of 5 mA / cm^2, cost of \$25 / m^2 and unassisted start from -20 °C [1]. These statistics are not yet competitive with the current version of the internal combustion engine. Therefore, the department of energy, or DOE, has come up with targeted goals for the PEMFC by 2010 and 2015. The targeted goals for 2010 / 2015 are shown in Table 1 [1]. These statistics are far more competitive with the internal combustion engine and can bring about the commercialization of PEMFC.

Table 1: DOE targeted goals for fuel cell membranes [1].

DOE technical targets for membranes

Characteristic	Units	2005 status	2010 target	2015 target
Operating temperature	°C	≤ 80	≤ 120	≤ 120
Inlet water vapor partial pressure	kPa	50	≤ 1.5	≤ 1.5
Membrane conductivity at inlet water vapor partial pressure				
Operating temperature	S cm-1	0.10	0.10	0.10
Room temperature	S cm-1	0.07	0.07	0.07
-20 °C	S cm-1	0.01	0.01	0.01
Oxygen crossover[a]	mA cm-2	5	2	2
Hydrogen crossover[a]	mA cm-2	5	2	2
Area specific resistance	Ω cm2	0.03	0.02	0.02
Cost[b]	$ m-2	25[c]	20	20
Durability with cycling				
At operating temperature ≤ 80 °C	h	~2000[d]	5000[e]	5000[e]
At operating temperature > 80 °C	h	Not available[f]	2000	5000[e]
Unassisted start from	°C	-20	-40	-40
Thermal cyclability in presence of condensed water		Yes	Yes	Yes

[a] Tested in MEA at 1 atm O_2 or H_2 at nominal stack operating temperature.
[b] Based on 2002 dollars and costs projected to high volume production (500,000 stack per year).
[c] Based on 2005 TIAX study and will be periodically updated.
[d] Steady state single cell durability is 25,000 h.
[e] Based on appropriate test protocol (to be developed).
[f] High temperature membranes are still in a development stage and durability data is not available.

The higher operating temperature resulting from the DOE targeted goals allows for a reduction in radiator size up to a 1/3 of the original size [1, 11]. The higher operating temperature also allows for less heat loss which eliminates need for complex humidification systems [1, 11]. Furthermore, low temperature fuel cells have several issues including low fuel impurity intolerance, high heat rejection, poor electrochemical kinetics, bad water management and require platinum containing catalysts [7, 12]. The uniform distribution of water is also important in fuel cell operation and directly correlates with the relative humidity which is dependent on temperature [3]. Platinum is expensive and the opportunity to use other materials could reduce costs. However, higher temperatures also result in the loss of mechanical durability and dimensional stability due to glass transition temperatures, T_g, of 80 to 120 °C [12, 13]. Tensile

strength, compression strength and puncture resistance all decrease at higher temperature [3]. Also, chemical degradation reactions accelerate at higher temperatures [3]. Higher temperatures also lead to platinum dissolution and migration under electrode potential cycling [11]. High pressure is needed to maintain hydration at high temperatures as well [7]. Electrode potential cycling is prevalent for fuel cells operating in a driving cycle. Platinum degradation and migration result in performance losses and degradation within the membrane including carbon corrosion and chemical attack [11, 14]. Hydrogen crossover is a major factor in mechanical durability and can accelerate at higher temperatures [3]. The formation of pinholes due to membrane degradation can result in large fuel crossovers [15, 16]. An image of a pinhole is shown in Fig. 2 [15]. Thus, durability issues in fuel cell membranes must be addressed especially at higher temperatures.

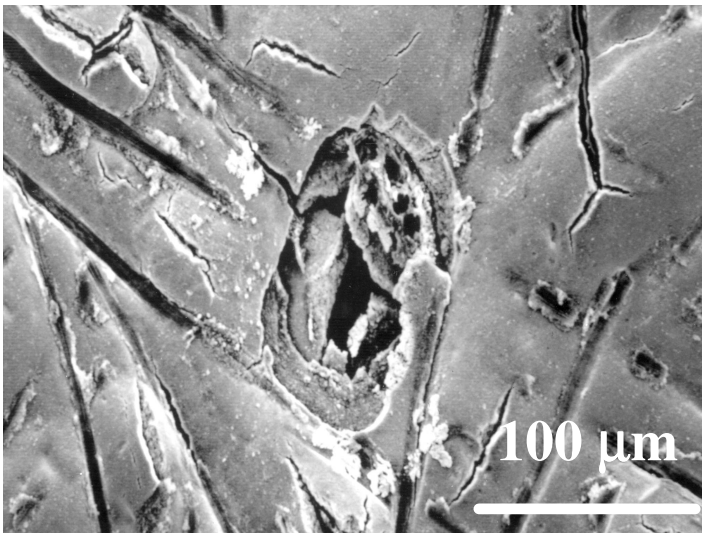

Figure 2: Image of pinhole in membrane. Reprinted with permission from [15]. Copyright 2008, The Electrochemical Society.

Proton exchange membranes, PEM, are subjected to cyclical hygro-thermal stresses during operation [9, 17, 18]. These hygro-thermal stresses result in the swelling and shrinking of the membrane during operation and cause performance drops as well as

degradation of the membrane [1, 8, 19]. The hygro-thermal stresses are the result of variations in temperature and humidity during operation that causes cyclic stresses and strains in the membrane [18, 20]. Mechanical failures resulting from hygro-thermal stresses include through-the-thickness flaws or pinholes and delamination between the membrane and the gas diffusion layers, GDL [17, 18]. Finite element modeling assuming some basic material responses has been used to model the effect of hygro-thermal stresses on the fuel cell membrane [17, 18]. From this modeling it has been found that hygro-thermal stresses create significant in-plane stresses within the membrane that lead to residual tensile stresses and eventually damage the membrane [17, 18]. Contour plots of the hygro-thermal stresses are shown in Fig. 3 [17]. These hygro-thermal stresses can create areas of high in-plane tensile residual stress in localized sections of the membrane [17, 18]. Since the purpose of the membrane is to split H_2 into electrons and protons and the subsequent transportation of protons, increases in conductivity must be achieved while minimizing water uptake and subsequent swelling [1]. This swelling, along with the subsequent shrinking, leads to the hygro-thermal stresses that can cause membrane failure.

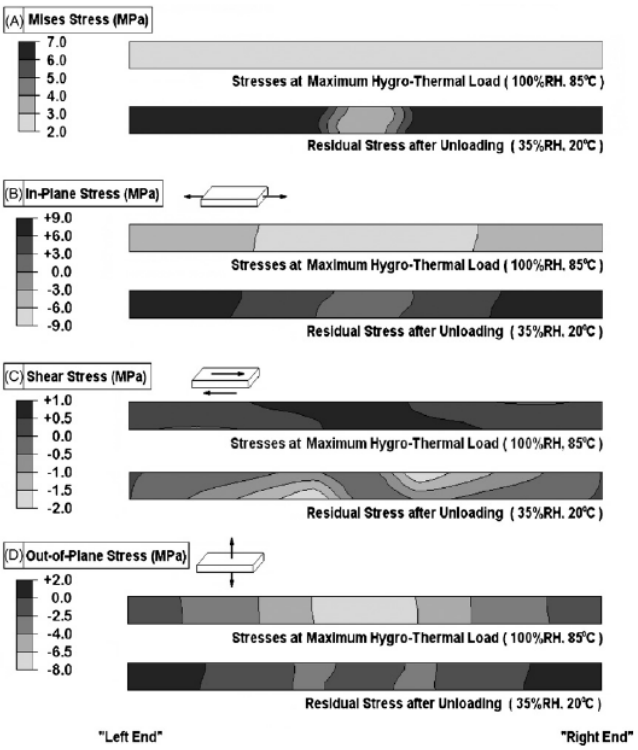

Figure 3: Contour plots of stresses in membrane from finite element modeling. Reprinted with permission from [17]. Copyright Elsevier Ltd.

PEMFC have degradation liabilities resulting from catalysts and support materials due to the decrease in electrochemically active surface areas, bipolar plates due to corrosion and membranes due to hydrogen peroxide (H_2O_2) attack [12, 21, 22]. The microstructure of the catalyst layers can change due to chemical degradation or mechanical failure under cycling [21, 22]. However the mechanisms of the microstructure changes in catalyst layers is not fully understood since mechanical damage can appear as flaws or mud-cracks, delamination between the carbon-catalysts agglomerate and the electrolyte, or corrosion of the carbon [21, 22]. It is certain, however, that cycling from hygro-thermal stresses resulting from the operating conditions of fuel cells in vehicles results in mechanical damage or degradation [21, 22]. One of the problems with fuel cells is that catastrophic failure in one cell can lead to the failure of the entire stack [20]. Membrane degradation tends to manifest itself as gradual

unrecoverable performance decay followed by sudden failure [2, 20]. Thus, the ability of the membrane to resist mechanical breach in the form of pinholes or tears is often the limiting factor in durability [20]. This membrane failure is believed to be the result of combined chemical and mechanical effects [8, 19, 20].

Extensive research has been conducted to elucidate the chemical pathways for membrane decomposition [20]. Electrocatalyst sintering degrades MEA due to thermal induced coalescence and growth following surface migration over carbon support material, and 'Ostwald ripening' which follows dissolution redeposition mechanisms [23]. Platinum particle agglomeration triggered by corrosion of carbon support also degrades MEAs [23]. Electrocatalyst poisoning, surface segregation and morphology changes due to the presence of strong chemisorption by species such as carbon monoxide, sulfur compounds, products of methanol oxidation, etc will degrade the MEA [23]. Degradation of the MEA is also a result of self segregation of elements in mixed metal oxides or alloys brought on by potential excursion, etc [23]. Degradation of ion conducting components, including the membrane and smaller aggregates present alongside the electrocatalyst in the reaction layer, due to the free radical species generated at the interface is also a factor [23]. All of these events are strong functions of operating conditions [23]. Hydrogen peroxide, H_2O_2, lead free radical attack and subsequent membrane degradation are of importance due to the potential of rapid irreversible damage [23-25]. H_2O_2 forms by the oxygen reduction reaction in the intermediate step at the cathode or by the crossover of oxygen from the cathode to the anode [23, 24]. Membrane degradation is initiated by Fenton type metal cation catalyzed decomposition of H_2O_2 [23, 24]. H_2O_2 damage results in the loss of repeating units and

the release of fluoride ions [23-25]. Bubbles form in the membrane after the free radical attack [24]. Fenton's test is the standard used to examine peroxide attack but does not accurately simulate the fuel cell operating environment [23]. Standard tests also result in non-uniform degradation due to differences in current density [25]. The best method for testing chemical degradation is the long-term test but this is expensive and impractical due to extensive time requirements [23]. Chemical degradation and mechanical fatigue have been shown to interact with one another [19]. This involves hydration that induces mechanical degradation and high potentials that accelerates chemical degradation and the presence of liquid water that enhances both [19].

On the other hand, there is a lack of systematic study and understanding of mechanical degradation as a result of chemical attack and relative humidity, RH, cycling [20]. It also has been shown that both chemical aging and RH cycling conditions can be realized at local regions of the PEM stack [19, 20]. While, fluoride ion emission rate (FER) and H_2 cross flux are typically used to examine degradation in membranes, they are not very indicative of the actual degradation a membrane experiences during operation [20, 26]. Voltage decay rate is a critical measure of the performance, and thus durability, of the membrane but, it does not indicate what is actually happening to the membrane itself during operation [20, 26]. Relative humidity has been shown to greatly affect yield stress and Young's modulus but, it has little effect on strain to failure [20]. Strain-to-failure is more indicative of the actual degradation of a fuel cell membrane during operation due to its sensitivity to localized degradation, chemical degradation and RH cycling [20]. RH cycling affects this strain to failure to a large extent [20]. Chemical attack on the membrane has a huge effect on strain to failure as well [20]. Membranes in

fuel cells need to be durable enough to withstand mechanical damage and as well as chemical degradation [27].

Recently, this durability issue has attracted more extensive attention [9, 28, 29]. Long term aging studies have been conducted to investigate the effects of operating conditions [2, 26]. Studies have shown that degradation is primarily due to the decay of MEA [28]. The early failures of membrane have been shown to be primarily structural failures [28]. This suggests that mechanical degradation, either by chemical or mechanical means, is the dominant mode of failure. Any type of discontinuity in the membrane reduces the performance and lifetime of a fuel cell [27]. Thus the membrane itself is a major source of failure [27].

The degradation mechanisms of fuel cell membranes are not clearly understood at this time [28]. What has been shown is that the fatigue strength of Nafion NR111 is 1/10 that of its tensile strength [28]. This highlights the effect of RH cycling on the mechanical durability of the membrane. RH cycling at constant temperature can be used to simulate the mechanical loading experienced by membranes during operation [27]. The cyclical stresses and strains from varying temperature and humidity also result in an increase in H_2 crossover over time [28]. Voltage also decays over time during cycling [26]. The mechanical fatigue of MEA has been shown to cause mechanical degradation of the membrane as well [9, 29]. Hydration, and to a lesser extent temperature, acts as the driving force for mechanical breach [27, 29]. Young's modulus, proportional limit stress and swelling due to water uptake influence the mechanical response of fuel cell membranes [9]. These factors are strongly dependent on environmental conditions such as temperature, humidity and water content [9]. The proportional limit stress is the

intersection of the tangent lines of the elastic and strain hardening slopes which are characteristics in PEM stress-strain curves [9]. The Young's modulus and proportional limit stress decrease greatly with increasing temperature while, the dimensional change increases significantly with rising temperatures [9]. In-plane tensile residual stresses contribute to mechanical failures as well [27]. All these factors can severely reduce operation lifetimes in PEMFC.

Systematic studies on both ex situ and in situ degradation modes have not been fully explored [30]. Failure modes and effects analysis (FMEA) is required to explore membrane durability [30]. Under this analysis, the causes explored include material properties, defects and fuel cell assembly; the failure modes to examine are thermal, chemical and mechanical; and the effects are fuel cell stability, power and lifetime [30]. There are several types of morphological anomalies which have a variety of effects. Cracks on the catalyst surface can lead to defect propagation to pinholes, increased resistance within catalyst layers, flooded areas, areas susceptible to catalyst erosion and areas with higher radical concentrations [15, 30]. Orientations and roughness of the membrane results in variable contact resistance, mechanical stress variations and less control over morphology [30]. Delamination between the catalyst layers and the bare membrane can result in the development of flooded areas, increased resistance in MEA, development of pinhole areas, loss of apparent catalytic activity and the development of areas susceptible to erosion [15, 30]. MEA delaminations have been observed at the anode and cathode interfaces of fuel cells [16]. Electro-catalyst surface area losses are due to platinum particle growth [11, 14]. Higher temperatures increase particle sizes during cycling [11, 14]. The presence of catalyst clusters reduces activity over the entire

active area and increases point activity [30]. Finally, variations in the thickness of the membrane may result in variable resistance throughout MEAs, areas susceptible to pinhole formation and mechanical weakness [30]. In Fig. 4, an image of a crack in the catalyst layer is visible [30]. An example of delamination in MEAs is shown in Fig. 5 [30]. Any of the previous defects can result in the failure of fuel cell membranes. However, while these PEMFC failure modes are receiving attention, less attention has been given to the causes and mechanisms of fuel cell degradation [2].

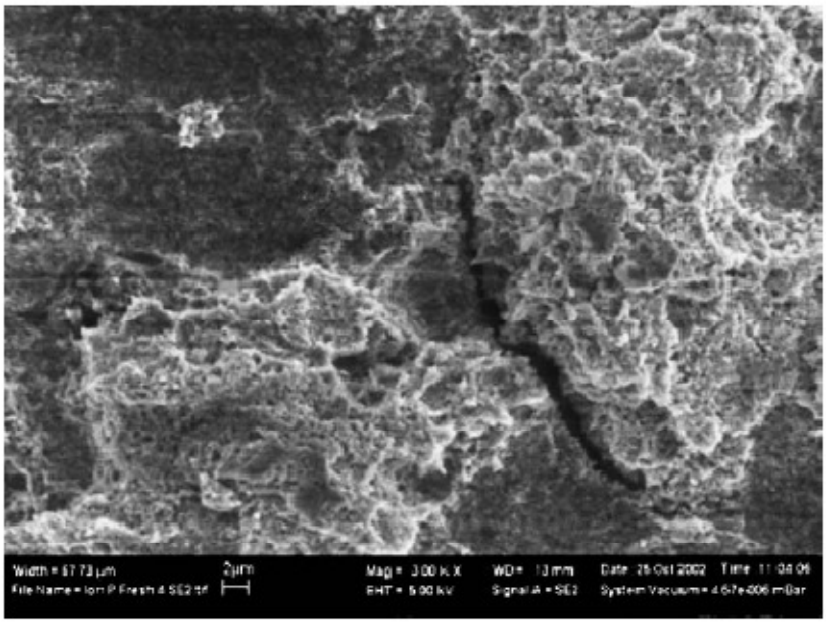

Figure 4: Image of a crack in the catalyst layer. Reprinted with permission from [30]. Copyright Elsevier Ltd.

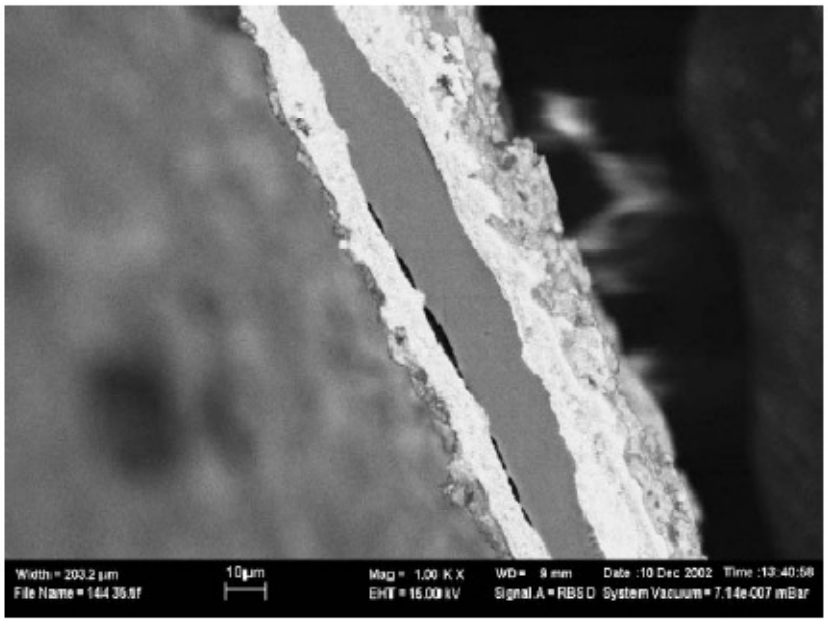

Figure 5: Image of delamination in MEA. Reprinted with permission from [30]. Copyright Elsevier Ltd.

The lack of investigation into the causes and mechanisms of fuel cell degradation can be attributed to a variety of reasons. One of the reasons is that there has been more focus on issues such as the initial operating requirements and PEMFC failure modes early in the development of fuel cells [2]. It has also been suggested that there was an underestimation of the severity of lifetime problems [2]. The membranes used in fuel cells ideally would be able to perform over the full range of the system operating temperatures with less than 5% performance loss at the end of life [2]. Several factors go into the durability of fuel cell membranes including impurities, subfreezing temperatures, load cycling from electrical potentials in fuel cells, fuel starvation and start / stop cycling [2]. The last factor, start / stop cycling, turns out to be very critical. This factor has been examined using in situ testing of the lifetimes and accelerated lifetimes of membranes [2]. This start / stop cycling behavior results in physical degradation including membrane creep, micro-crack fracture and structural / morphological changes [2]. The chemical

degradation further exasperates the damaging of the membranes [2]. Other issues include the electro-catalyst layers' stability and transportation issues with gas diffusion layers [2]. However these factors pale in consideration of chemical degradation and in mechanical degradation, which can exasperate the chemical attacks on the membrane.

There are several avenues that can be pursued in order to improve membrane durability. Suitable heat treatment of catalyst layers can suppress degradation [16]. Delamination can be suppressed by optimizing the MEA preparation conditions [16]. Long hot pressing durations result in significantly better durability but this does not result in any significantly improved performance [16]. Edge protection films have been incorporated into MEA systems to improve durability [8]. The resulting reinforced MEA samples had longer lifetimes as well as equally as good performance when compared to unreinforced MEA samples [8]. A graph comparing the lifetimes of MEA and edged protected MEA is shown in Fig. 6 [8]. MEA samples have also been reinforced by incorporating a tougher layer in-between the bare membrane layers such as in Gore-Select's reinforced Nafion membrane [3, 8]. However, a greater understanding of how membranes fail is needed to truly improve durability.

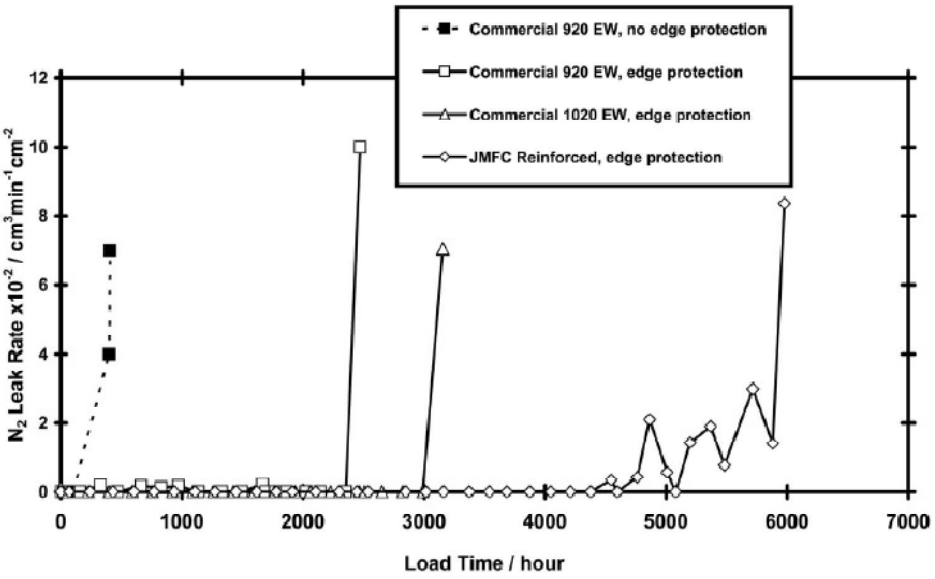

Figure 6: Comparison of lifetimes of various MEA samples. Reprinted with permission from [8]. Copyright 2008, The Electrochemical Society.

Crack initiation mechanisms in polymers are not completely understood [27]. Fatigue crack growth rate is governed by the stress amplitude and the stress level [27]. Stress gradients can develop from membrane bending due to delamination [27]. Investigating the cracking behavior in membranes will help in the isolation of issues in membrane durability. The principal issues governing coating fracture include constitutive relations for coating material, stress transfer form substrate to coating and disorder of coating and interface properties [31]. Strength irregularities greatly influence crack patterns [31]. These crack networks are influenced by the stress state in coatings and the anisotropy of coating and substrate mechanical properties [31]. The properties of coatings and interfaces are greatly dependent on the strength and toughness of the coating and the adhesive strength and toughness of the coating-substrate interface [32]. Common tests of these properties are peel tests, scratch tests, indentation tests and tension or fragmentation tests [32]. The crack density plateau or saturation level is a measure of

adhesion between the coating and the substrate [32]. This shows how the adhesive properties of MEAs can be quite critical. A number of approaches may be used for the modeling of cracks including linear-elastic, shear-lag, fracture mechanics, stress based ideas, elastic or elastic-ideal plastic behavior, cohesive zones and finite element techniques [13, 32].

Another method that can be used to address membrane durability is the imaging of membranes through microscopy. Microscopy provides information on the origin(s) of failure, crack propagation direction, location of arrest lines, the identification of different regions and an overview of the fracture surface [33]. Thus microscopy complements the examination of cracks in determining failure behavior. SEM, scanning electron microscopy, provides large depth of field and high resolution [33, 34]. However, observations of fracture surfaces are not always sufficient [33]. They can determine the location and type of defect, but not necessarily the time at which the membrane failed or which specific defect(s) led to this failure.

Polymers can fail at relatively low stress levels due to long-term stresses (creep rupture), cyclic stress (fatigue), presence of structural flaws and stress-cracking agents (environmental stress cracking, ESC) [34]. Polymers such as PEMs are notch sensitive, temperature sensitive, susceptible to chemical degradation and ESC factors such as exposure to chemicals and temperature over time [34]. Adhesion issues within the MEA can also be an issue. Mechanical adhesion, physical adhesion and chemical adhesion must be examined to determine the strength of the interface between the catalyst layers and the bare membrane [34]. Other issues that can present problems include voids, blisters and surface defects [15]. Thus, more insight needs to be gained on the causes and

mechanisms of mechanical degradation within the membrane along with the examination of cracks and surface defects. Mechanical testing can be used to analyze failure and characterize material behavior such as fracture resistance [35].

Focus of Research

The testing procedure that will be used to examine the mechanical degradation and corresponding defects in fuel cell membranes will proceed as follows. Biaxial mechanical testing of the membranes; imaging of membranes before and after testing; detection of leaking after testing; determining the effect of environmental conditions, specifically temperature, on membranes; and characterizing defects present within the catalyst layers will provide the necessary details needed to examine the durability issues. A mechanical fixture will be used to mimic the stresses a membrane experiences from the swelling and shrinking encountered during the operation of an actual fuel cell [36-45]. The mechanical fixture creates biaxial mechanical stresses in a cyclical manner through pressurization of the membrane in a blister like fashion [36-39, 42, 44, 45]. Imaging of the membrane before and after testing will help describe the damage and failures developed during the mechanical testing of the membrane. Leaking of the membrane is the most critical failure criteria since any defect in the membrane will result in significant performance loss and accelerate the failure of the fuel cell membrane. A bubble point testing fixture will be used to detect any leaking of the membrane after testing and indentify areas of interest to image. Temperature has a large effect on membrane behavior and durability and will need to be examined carefully. The characteristics of defects, as well as how they form, grow and / or travel, need to be determined in order to analyze their effect on membrane degradation.

A potential key issue in the mechanical degradation of membranes, and the focus of this research, is the occurrence of stress concentrations or localized stresses. These tests will help determine the location of stress concentrations, how stress concentrations are formed and how stress concentrations lead to failure or weakening of the membranes. Once the localization of stresses has been identified and characterized, models can be developed that predict the lifetime of fuel cell membranes under various conditions and circumstances. This information will help determine which membranes will prove to be the most durable and best performing materials for use in commercial fuel cells.

Chapter 2: Volume-Controlled Blister Fixture Testing

Abstract

Long-term durability of the membrane electrode assembly (MEA) in proton exchange membrane (PEM) fuel cells is one of the major technological barriers to the commercialization of fuel cell vehicles. The cracks in the electrode layers of the MEA, referred to as mud cracks, are potential contributors to the failure in the PEM. To investigate how these mud cracks affect the mechanical durability of the MEA, pressure-loaded blister tests are performed at 90°C to determine the biaxial fatigue strength of Gore-Primea® Series 57 MEA. In these volume-controlled tests, leaking rate is determined as a function of fatigue cycles. Failure is defined to occur when the leaking rate exceeds a specified threshold. Post-mortem characterization using bubble point testing and FESEM (field emission scanning electron microscopy) was conducted to provide visual documentation of leaking failure sites. Analysis of the experimental leak test data indicates that the MEA has much shorter lifetimes at same nominal stress levels than membrane samples without the electrode layers. FESEM photomicrographs of leaking locations identified via the bubble point testing show cracks in the membrane that are concentrated within the mud cracks of the electrode layer. These two pieces of information indicate that the mud cracks within the electrode layers contribute to the leaking failures of the MEA assembly. For the fuel cell industry, this study suggests there is an opportunity to reduce the likelihood of membrane pinhole failures by reducing the size and occurrence of the mud cracks formed during the MEA processing or by increasing the fatigue resistance (including the notch sensitivity) of the membrane material within the MEA.

Keywords: Fuel cells, membranes, mechanical behavior, fatigue lifetimes, failure, blister test, proton exchange membranes, polymer electrolyte membrane, PEM, membrane electrode assembly, MEA, catalyst layer, electrode cracks

Introduction

In order to analyze the durability of membranes, a volume controlled blister fixture was used to mechanically fatigue MEA and PEM samples. The volume controlled blister fixture (described in the next section) allows for the pressurization of membranes in a blister configuration. This blister configuration, under cyclical pressurization, mechanically simulates the shrinking and swelling behavior of fuel cell membranes during operation in a motor vehicle. The volume controlled blister fixture allows for the control of the loading profile in terms of amount of time under load, magnitude of the load and the number of cycles of loading and unloading. The volume controlled blister fixture is placed in an oven in order to control temperature. The data resulting from the volume controlled blister fixture is reduced to determine MEA and PEM lifetimes. To achieve more precise lifetimes, a leaking model was developed to further reduce the data from the volume controlled blister fixture. This provided more accurate information of when leaking occurs. After the testing, bubble point testing and FESEM imaging was conducted to examine the leaking sites to gain a better understanding of the behavior of MEAs during mechanical fatigue.

Experimental Procedure

Mechanical fatigue apparatus

A volume-controlled blister fixture was used to examine biaxial fatigue of the MEA. This fatigue fixture consists of a stainless steel block with ten evenly spaced 19

mm diameter cylindrical chambers, each with inlet and outlet valves. Only eight of the chambers were used for testing. Teflon backing material is placed between the MEA or PEM and the top of the steel block for sealing purposes. Teflon gaskets are placed within the top steel plate on top of the MEA or PEM for further sealing. The Teflon backing and gaskets also prevent rubbing and wear between the membranes and the steel apparatus. Each chamber is pressurized by a charged volume of air, and spring loaded pistons are used to control the volume changes that the membrane blisters over each chamber experience. The springs limit the travel of the pistons and washers are added to limit the distance the pistons travel even further. Each set of chambers represents one particular pressure level. The fixture is placed in an oven at a controlled temperature and nominal humidity of 3% RH (uncontrolled). The chamber pressure is then cycled to subject samples to cyclic stresses. Periodically; the 4-200 s, the 4-20 s and the 4-4 s cycled samples (described at the end of this section) are subjected to pressure drop measurements which are used to calculate leaking rates. In these tests, the chambers are pressurized to a fixed volume, and subsequent pressure decay is measured over a period of 20 seconds followed by 20 seconds of recovery. Additional details on the blister fatigue testing are available in references [36-39, 42, 44, 45]. Two diagrams of the blister fixture are shown in Fig. 7 and Fig. 8.

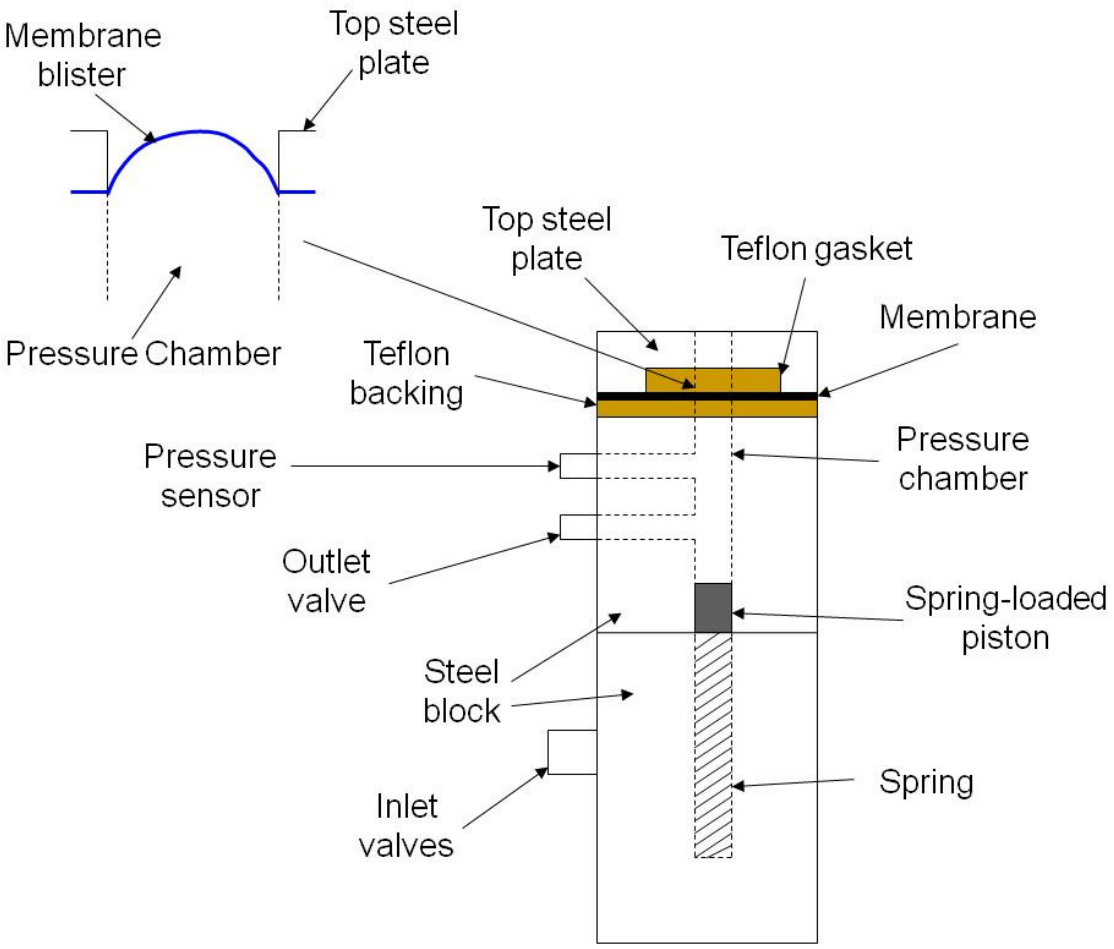

Figure 7: Cross section of mechanical fatigue apparatus.

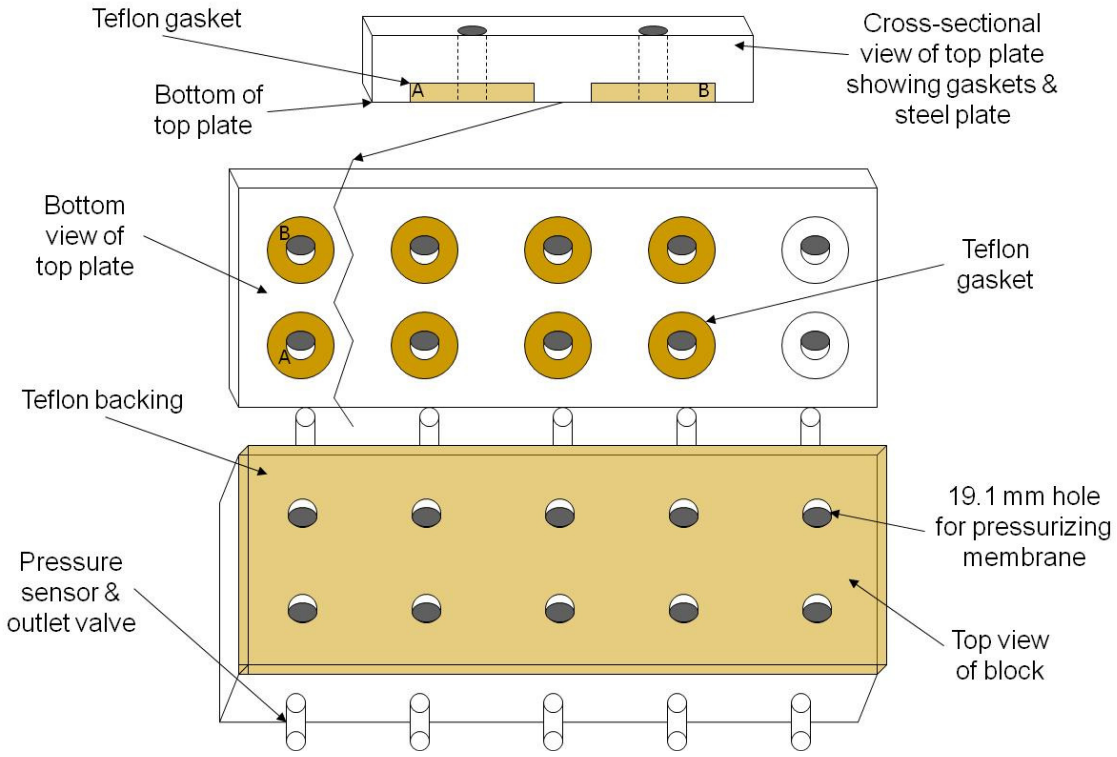

Figure 8: View of plate and block of mechanical fatigue apparatus.

MEA samples for the present blister testing came from Gore-Primea® Series 57 MEA sheets. The Gore MEA sheets are commercially available. Each fatigue test of the MEA was conducted at 90 °C using pressurized-unpressurized cycling of 200-4 s, 20-4 s, 4-4 s, 20-20 s, 100-100 s, 4-20 s and 4-200 s. In our notation, 20-4 s cycling refers to samples that were pressurized for 20 seconds, followed by 4 seconds unpressurized. In this way, we are able to examine the effects of duty cycle on the leaking behavior of the MEA.

Leak site detection apparatus

To determine the location of leaking sites, bubble point testing was also conducted. In these tests, the tested MEA samples are removed from the fatigue testing block and are sealed in a fixture where each blister is submerged under water and air is used to pressurize each individual membrane blister from underneath. The bottom block

contains side air inlet valves that continue through channels in the block and up into eight exit holes on the top of the bottom block underneath each blister of the MEA samples. The top block contains eight 25 mm holes through its thickness. Screws surrounding each hole are used to secure each section tightly together. Leaking sites are visualized by the formation of air bubbles on the blisters as the air passes through damaged sites in the membrane. This is a simple and convenient way to determine the location of leaking sites within a blister. A diagram of the bubble point testing apparatus is shown in Fig. 9.

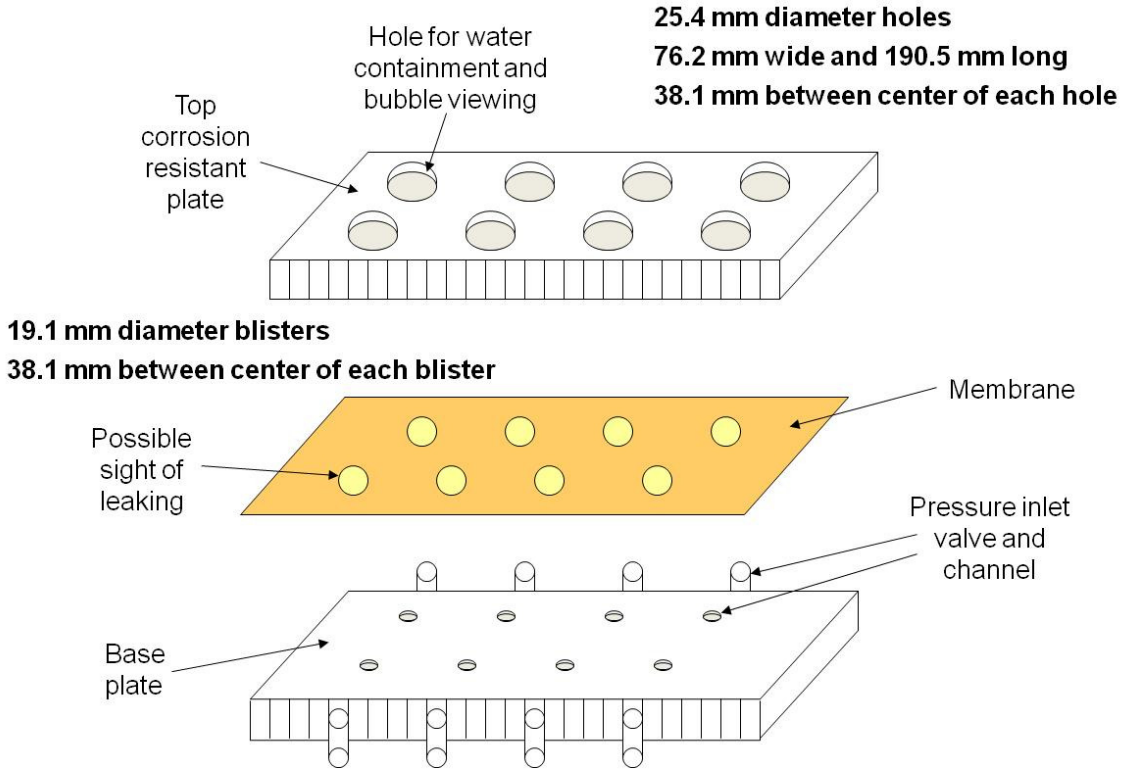

Figure 9: Diagram of bubble point testing apparatus.

Imaging apparatus

A LEO (Zeiss) 1550 Schottky field emission SEM (FESEM) was used to image tested MEA samples in order to examine failure sites. Both untested and tested samples were examined for comparison purposes. The bubble point testing results were used to determine which areas of the sample blisters are to be examined in the FESEM.

Volume-Controlled Blister Fixture Data

Typical data obtained from the blister mechanical testing fixture are shown in Fig. 10, Fig. 11 and Fig. 12. These data consist of the maximum and minimum pressures during a volume-controlled pressurization cycle versus the time at the beginning of the pressurization period. The pressures displayed in the legend refer to the nominal maximum pressure at the beginning of each test and to the nominal minimum pressures at the end of each test. A simple example of this is shown in Fig. 10 including a highlight of the region when the onset of leaking occurs. In this figure, the largest maximum pressure was 15.05 kPa with the maximum and minimum pressures for each subsequent cycle shown by separate curves. During the course of the fatigue test, the maximum and minimum pressures during a cycle decreased as a result of the viscoelastic response in the MEA. However, because these values are nearly identical for times less than approximately 18,000 seconds, we do not believe that leaking has begun to occur yet. (This is verified by subsequent analysis.) After this point, we note substantial differences in the maximum and minimum pressures, attributable to leaking that occurs. Naturally, this response is a function of the volume introduced into each blister, which in turn affects the initial pressure value. Figure 11 and Fig. 12 show the general trends of MEA samples at various nominal maximum pressures. The steady reduction in minimum pressure indicates that leaking is occurring whereas the ability to maintain respectable maximum pressures indicates that the scale of the leak is quite small, indicating that the membrane has not undergone catastrophic rupture. Again, the ability to induce and detect leaks rather than physical separation is believed to link this test to fuel cell failure modes. For the 20-4 s cycling, the MEA is pressurized for 20 s and then recovers for 4 s

before the next cycle begins, while for the 4-20 s cycling, the MEA is pressurized for 4 s and then recovers for 20 s before the next cycle begins. For tests such as the 4-20 s cycling, a separate leaking test corresponding to 20 s pressurized followed by 20 s recovery is conducted every 100 cycles to better analyze the amount of leaking over time due to the short pressurization periods of the main test. Figure 10 and Fig. 11 show more scatter due to the fact that all pressure cycles are plotted. Figure 12 shows less scatter due to the fact that only the leak test cycles ever 100 cycles are shown. These pressure measurement graphs provide an indication of the onset of leaking, but do not, by themselves, provide a quantitative estimate of the amount of leaking that is occurring to enable a precise definition of failure. For this, an analytical method for modeling the leaking is needed.

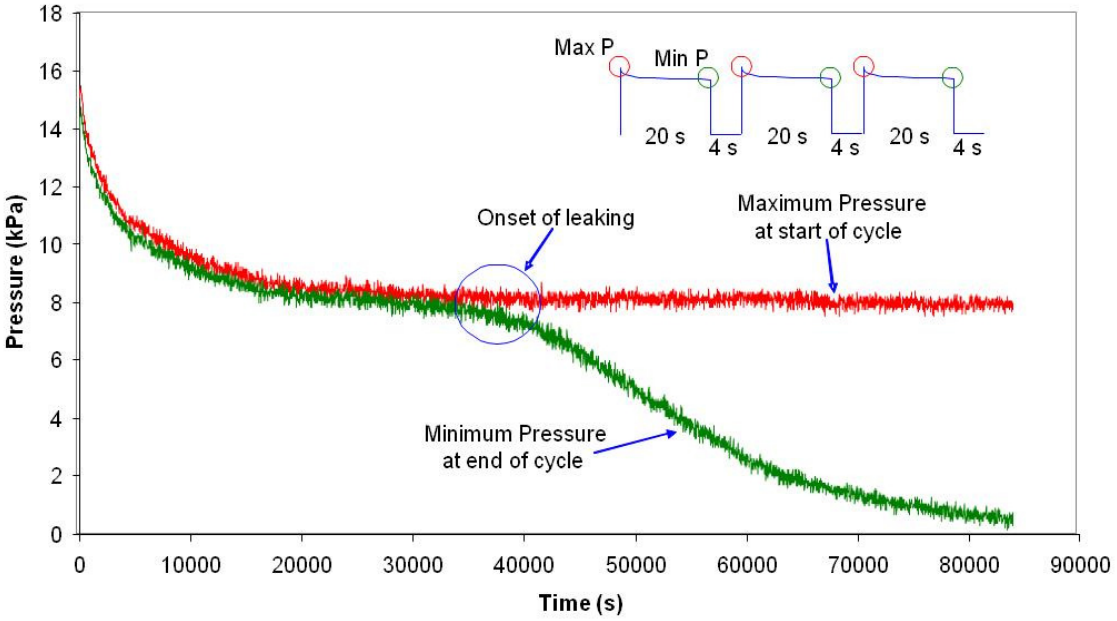

Figure 10: Gore MEA at 90 °C under 20-4 s cycling in the blister fixture.

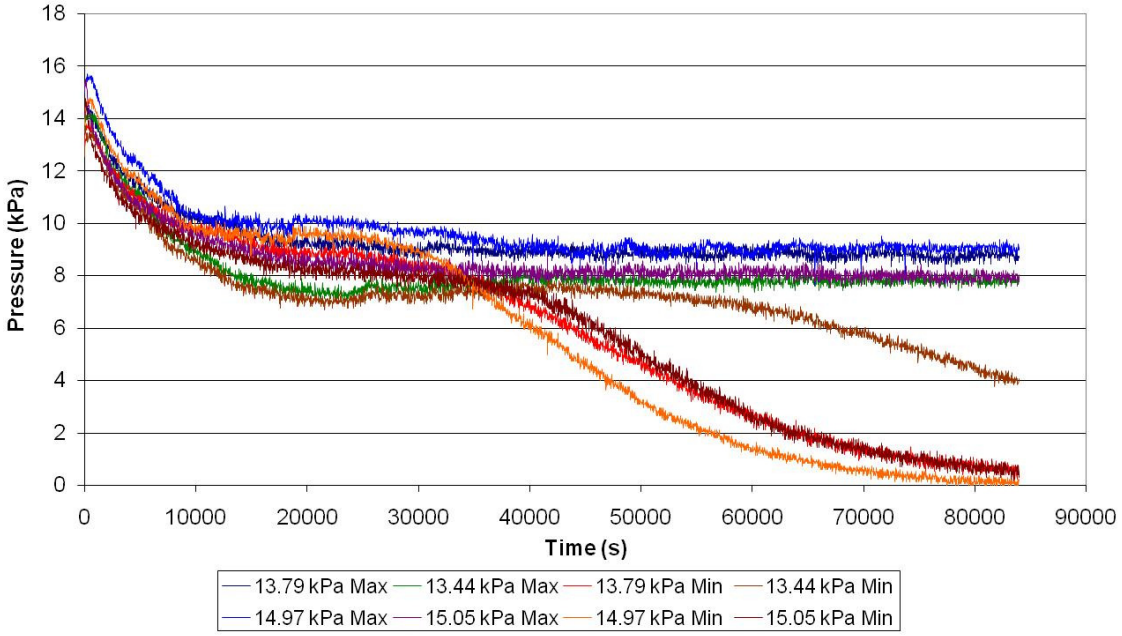

Figure 11: Results from four Gore MEA samples tested at 90 °C under 20-4 s cycling in the blister fixture.

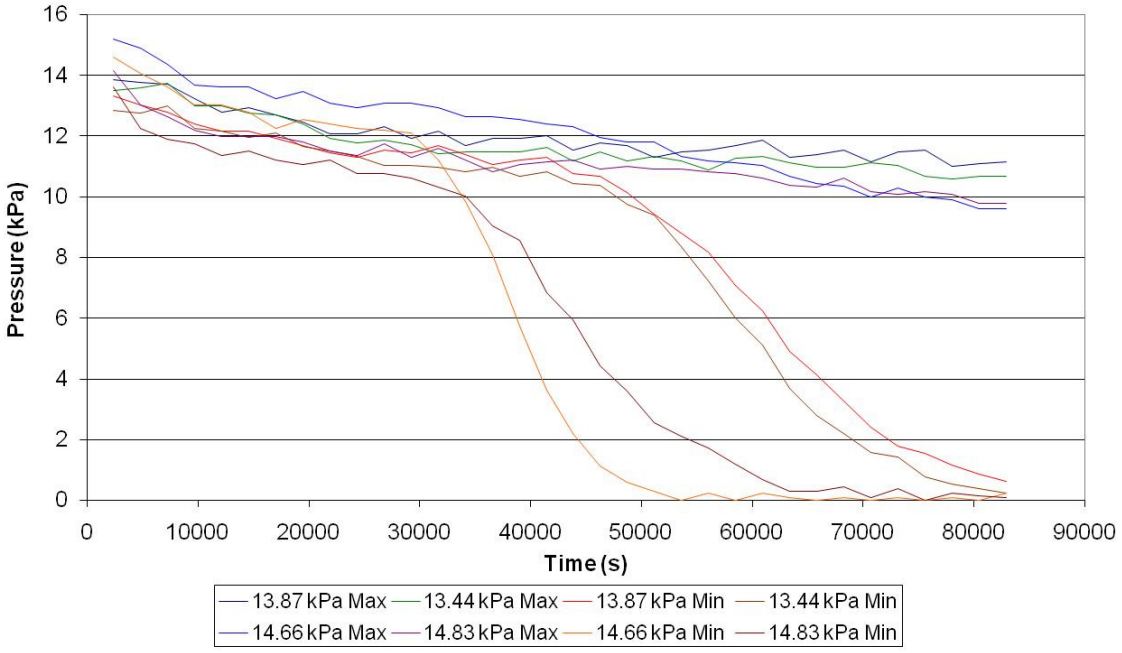

Figure 12: Results from four Gore MEA samples tested at 90 °C under 4-20 s cycling in the blister fixture.

A model of leaking rate

In our simple leaking rate model, we begin by considering the mass inside the blister chamber at any instant in time. This mass is given by

$$m(t) = \rho(t)V \qquad (1)$$

where *m(t)* is the mass inside the blister, $\rho(t)$ is the density of the air inside the blister, and *V* is the volume of the blister plus the piston chamber. Calculations estimate that the volume in the chamber is 7.24 cm^3 while the volume in the blister is 0.125 cm^3 for a pressure of 14 kPa and 0.105 cm^3 for a pressure of 10 kPa. Thus, the blister volume is negligible compared to that of the chamber volume. If we differentiate equation (1) with respect to time and assume that the total volume is nearly constant, we find that the change in mass inside the blister is given by

$$\frac{dm}{dt} = \frac{\rho_{STP}}{p_{STP}}\frac{T_{STP}}{T}V\frac{dp}{dt} + \frac{\rho_{STP}}{p_{STP}}\frac{T_{STP}}{T}p\frac{dV}{dp}\frac{dp}{dt} \approx \frac{\rho_{STP}}{p_{STP}}\frac{T_{STP}}{T}V\frac{dp}{dt} \qquad (2)$$

where the subscripts *STP* refer to standard temperature and pressure. (In such an approach, we assume that changes in total volume, blister plus chamber, due to changes in pressure are insignificant.)

We next relate the volumetric flow rate, *Q*, to the pressure gradient across the membrane on the basis of Darcy's law (assuming quasi-steady flow). In such a case, the volumetric flow rate across the membrane is given by

$$Q = -\frac{\kappa A}{\mu}\frac{(p - p_{oven})}{h} \qquad (3)$$

where κ is the permeability, *A* is the cross-sectional area of the membrane, μ is the viscosity of the air, *p* is the pressure inside the blister, p_{oven} is the atmospheric pressure of

the oven into which leaking occurs, and h is the thickness of the membrane. The mass flux rate out of the blister is then calculated as

$$\begin{aligned}\frac{dm}{dt} &= \rho Q \\ &\approx -\frac{\rho_{STP}}{p_{STP}}\frac{T_{STP}}{T}\frac{(p+p_{oven})}{2}\frac{\kappa A}{\mu}\frac{(p-p_{oven})}{h}\end{aligned} \quad (4)$$

where the density is approximated as the average density inside the blister and inside the oven.

If we equate the two expressions for the rate of change of mass inside the blister (equations (2) and (4)), we find that

$$\frac{dp}{dt} = -\frac{\kappa A}{\mu h V}\frac{(p-p_{oven})(p+p_{oven})}{2} \quad (5)$$

Equation (5) is integrated subject to the initial condition $p(0) = p_0$ to obtain

$$p(t) = p_{oven}\frac{p_0 + p_{oven} + (p_0 - p_{oven})e^{-\frac{\kappa A p_{oven}}{\mu h V}t}}{p_0 + p_{oven} - (p_0 - p_{oven})e^{-\frac{\kappa A p_{oven}}{\mu h V}t}} \quad (6)$$

or in its linearized form

$$\ln\frac{p-p_{oven}}{p+p_{oven}} = -\frac{\kappa A p_{oven}}{\mu h V}t + \ln\frac{p_0 - p_{oven}}{p_0 + p_{oven}} \quad (7)$$

For a particular test run at constant temperature, the coefficient of t in equation (7) is the slope in the linear regression and depends only on the permeability, κ. In our subsequent discussions, we define this term as $1/\tau$, so that

$$\frac{1}{\tau} = \frac{\kappa A p_{oven}}{\mu h V} \quad (8)$$

Here, $1/\tau$ represents the leak rate and τ can be thought of as a characteristic time in the leaking process. This provides a more robust measure of the leaking rate compared to

simply measuring it from a selected portion of the pressure drop values obtained by testing. In addition, the quality of fit of the model provides an indication of whether or not leaking is occurring. If the model does not fit well, then it is likely that changes in pressure are due to membrane viscoelasticity, or other factors, rather than leaking.

A consistency check is shown in Fig. 13. In this consistency check the leaking model term is used to back-calculate the pressures (leaking model curve) in the blister during the cycle where $1/\tau$ was calculated. This back-calculated pressure is then compared to the actual pressures in the blister recorded during testing (data curve). It can be seen from Fig. 13 that the leaking model pressures agree very well with the actual pressures in the blister during testing showing consistency.

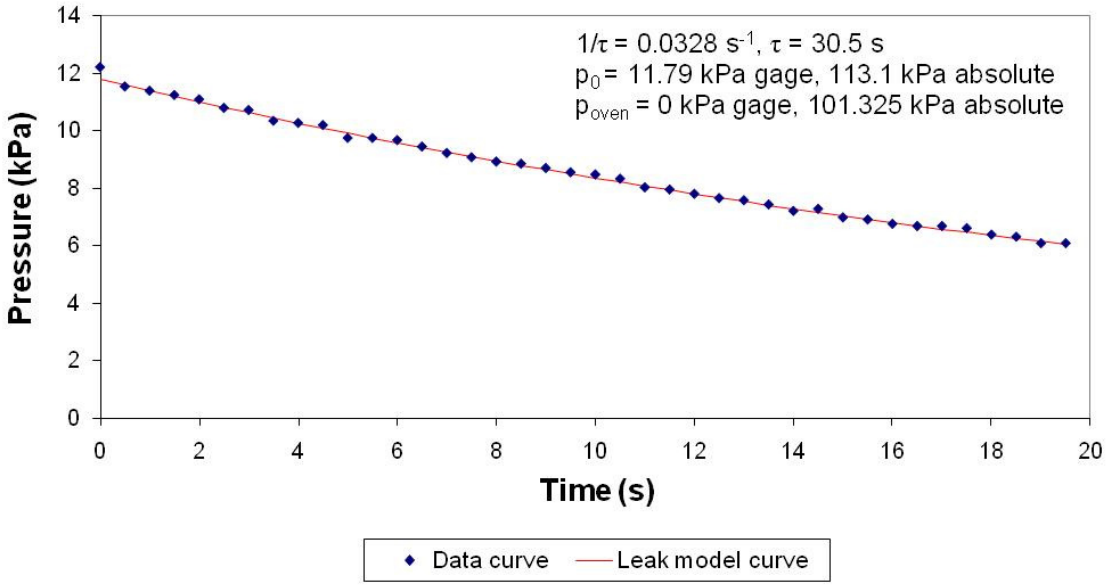

Figure 13: Leaking rate model consistency check plot.

Data Analysis

The calculated values for $1/\tau$ for Gore MEA samples tested at 90 °C under 20-4 s cycling and 4-20 s cycling, respectively, are shown in Fig. 14 and Fig. 15. It can been seen that analyzing leaking and defining failure due to leaking is easier by looking at Fig.

14 and Fig. 15 than it is by analyzing Fig. 11 and Fig. 12. For comparison purposes, we define failure as $1/\tau = 0.05\ s^{-1}$, or a characteristic time of 20 s, which corresponds to the pressurization and recovery times of a leaking rate test. The pressure drop during the 20 s of pressurization should be significant if the sample is to fail. If we compare the times where the leaking rate slopes rise exponentially in Fig. 14 and Fig. 15 to the point where the pressure begins to drop in Fig. 11 and Fig. 12, you will see that they occur at the same time for each sample in both cases. The severity of the slopes in Fig. 14 and Fig. 15 correspond well to the degree of pressure drop in Fig. 11 and Fig. 12 as well. Using both the pressure versus time and the leaking rate over time graphs, comparisons can be made between MEA and PEM samples and between MEA samples under different duty cycle ratios.

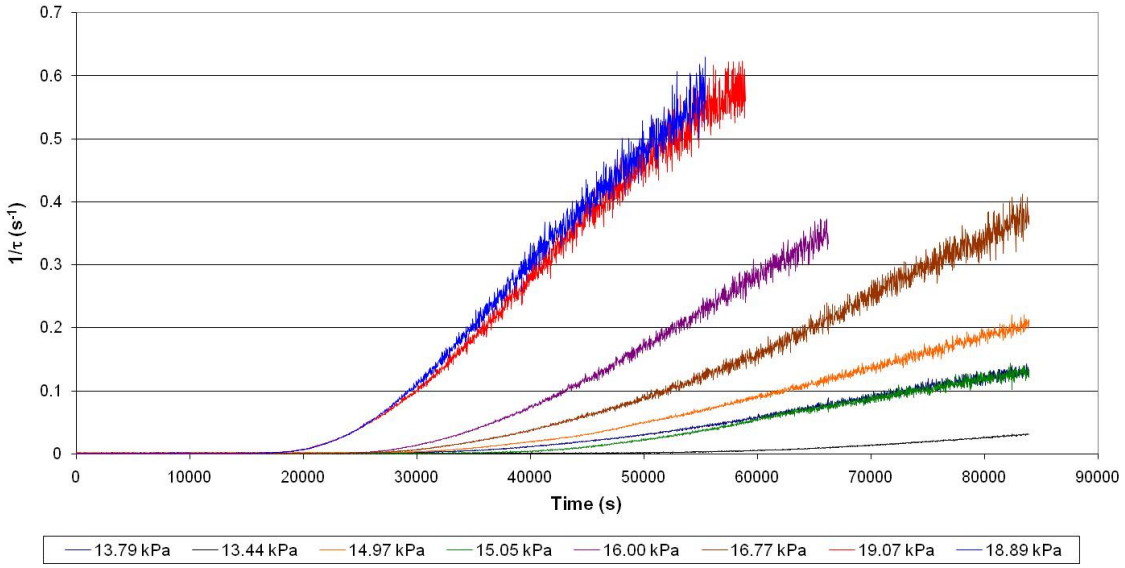

Figure 14: The reciprocal relaxation time results for the 20-4 s cycling data of Fig. 11.

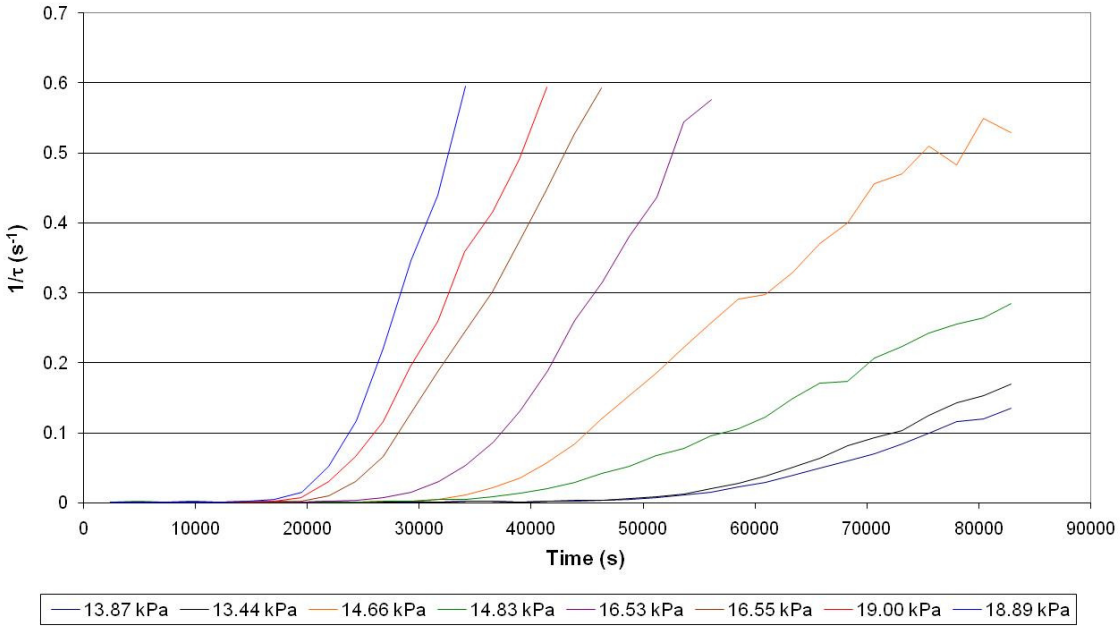

Figure 15: The reciprocal relaxation time results for the 4-20 s cycling data of Fig. 12.

Gore PEM versus Gore MEA

Shown in Fig. 16 and in Fig. 17, the nominal maximum stress encountered in PEM and MEA samples are plotted versus total time and versus number of cycles, respectively. The nominal pressure and nominal stress are related by Hencky's solution:

$$\sigma_r = \sigma_\theta = \frac{B_0}{4}\sqrt[3]{\frac{Ep^2a^2}{h^2}}$$

where B_0 is a constant that equals 1.724 for a Poisson's ratio of 0.4, E is the elastic modulus (46.5 MPa for Gore MEA and 24.6 MPa for Gore PEM at 90°C), p is the pressure in the blister, a is the radius of the blister (9.525 mm) and h is the thickness (0.042 mm for Gore MEA and 0.018 mm for Gore PEM). The elastic modulus values were obtained using DMA long term stress relaxation instantaneous modulus values under dry conditions. The initial maximum pressure for each sample was converted to its corresponding nominal maximum stress. Figure 16 and 17 both show that the PEM samples at a given failure time (test time or number of cycles) have higher stresses than

the MEA samples at the same failure time. Meaning MEA samples fail at lower stresses than PEM samples given a similar time frame. For Fig. 16 and Fig. 17, the total time / number of cycles corresponds to the time / number of cycles at which $1/\tau = 0.05\ s^{-1}$ for each sample, or the leaking rate failure criteria described previously.

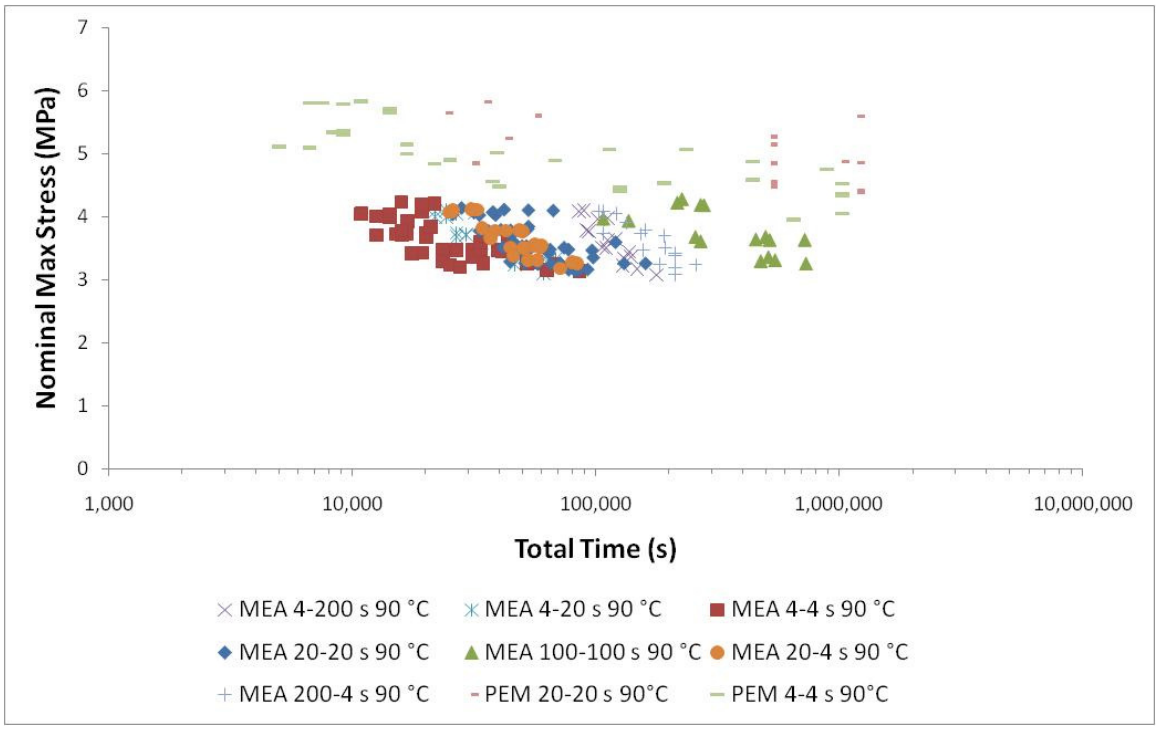

Figure 16: Comparison between Gore PEM and MEA at 90°C under various cycling.

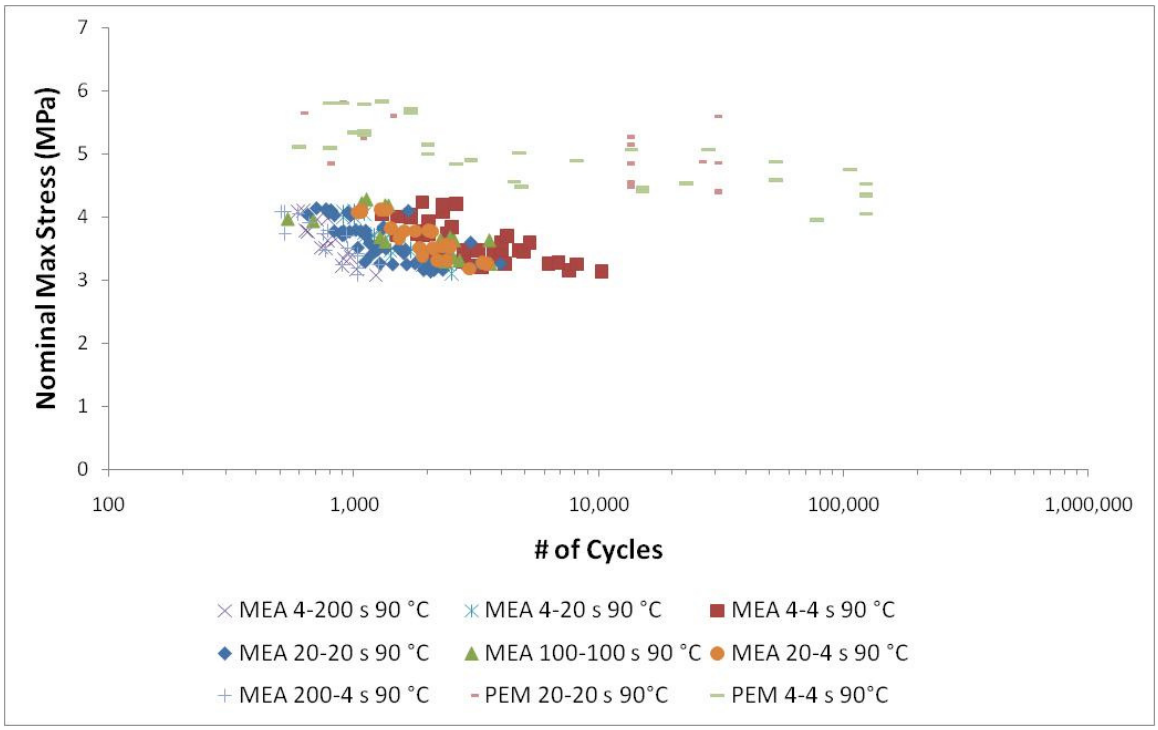

Figure 17: Comparison between Gore PEM and MEA at 90°C under various cycling.

Comparison between various MEA cycling ratios

In Fig. 16 and Fig. 17, we illustrated the nominal maximum stress versus the total time / number of cycles required for leaking failure (defined as $1/\tau = 0.05\ s^{-1}$). The results in this case do not appear to arrange themselves in any particular order. As an alternative way of examining the data, we considered the possibility that only the net time of loading (pressurization) influenced the failures. Thus, the MEA data in Fig. 16 and Fig. 17 are replotted in Fig. 18 as a function of net time at loading before failure. When the data are presented in this fashion, we see a clear trend: samples with short pressurization periods and long recovery periods (4-200 s and 4-20 s) tend to fail much sooner than samples with long pressurization periods and short recovery periods (20-4 s and 200-4 s). The other series with equal pressurization and recovery periods (4-4 s, 20-20 s and 100-100 s) fall somewhere in-between. A possible explanation is that samples with short pressurization and long recovery tend to maintain higher stresses longer than

samples with long pressurization and short recovery. With the long recovery periods, the membrane is effectively stiffer, resulting in a larger radius of curvature in the pressurized state and a correspondingly higher stress level. This results in leaking occurring sooner in short pressurization samples than in long pressurization samples. Again, the other sample series with equal pressurization and recovery times fall somewhere in-between.

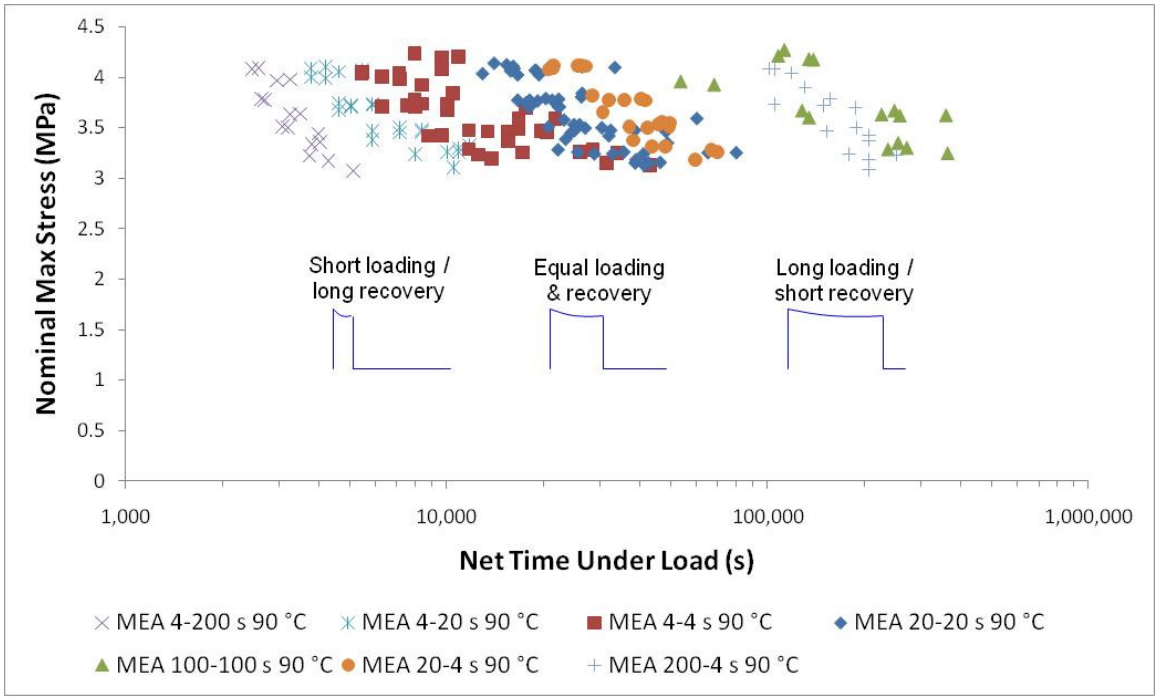

Figure 18: Comparison of various cycling ratios using leaking rate failure criteria.

Bubble point testing data

The bubble point testing performed on failed specimens has shown that for the MEA blister fatigue tests, the samples subjected to short pressurization and long recovery samples tend to leak near the center of the blisters (where the stress is expected to be the largest, and equal biaxial), while the long pressurization and short recovery samples tend to leak along the edges of the blisters (where the stresses are expected to be smaller and more uniaxial). Samples with equal pressurization and recovery periods tend to initiate leaks across the pressurized blister region. To illustrate this behavior, images of this

bubble point testing behavior are shown in Fig. 19, Fig. 20, and Fig. 21 for samples with long pressurization and short recovery, equal pressurization and recovery, and short pressurization and long recovery, respectively. In these figures, the 19-mm diameter circle corresponds roughly to the outer edge of the blister during the fatigue tests (the "grip" region). By using a larger diameter opening in the bubble point testing, we can identify leaks that occur in this region as well as in the center region.

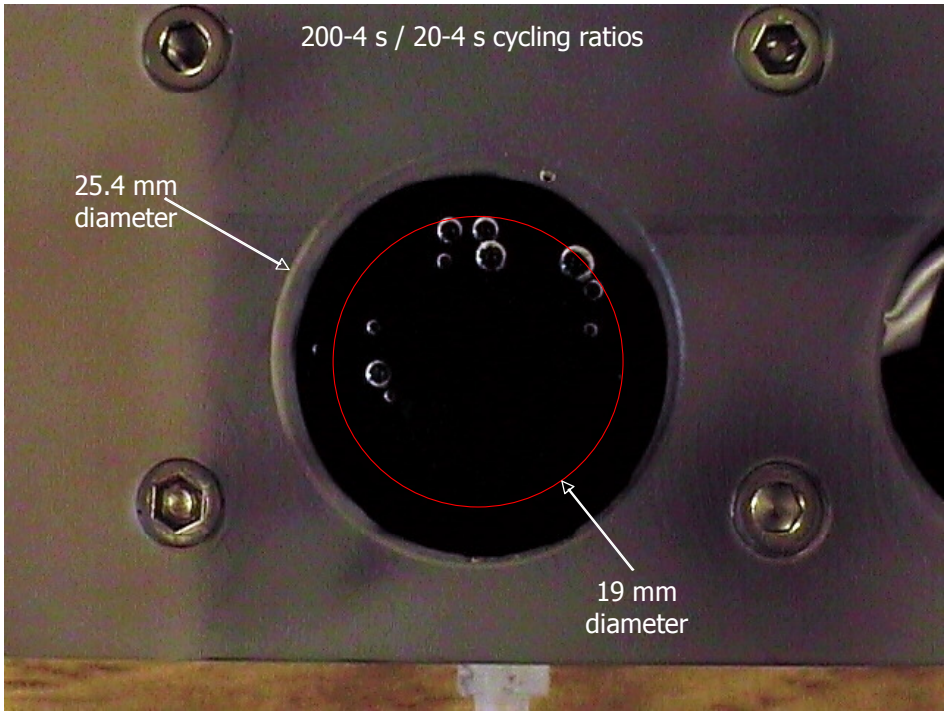

Figure 19: A characteristic bubble point test image of MEA at 90 °C.

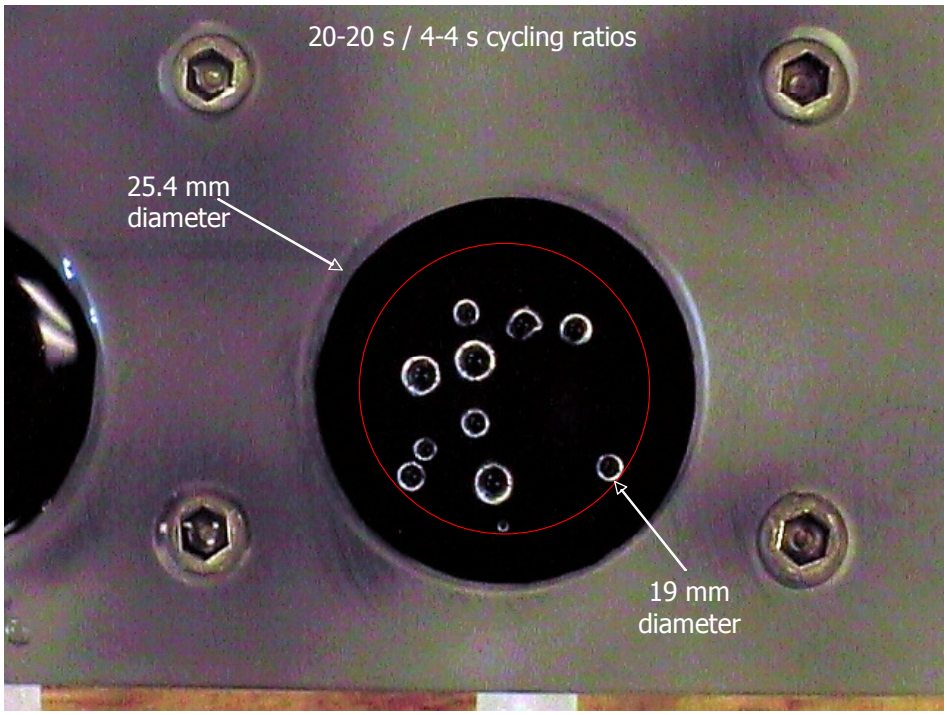

Figure 20: A characteristic bubble point test image of MEA at 90 °C.

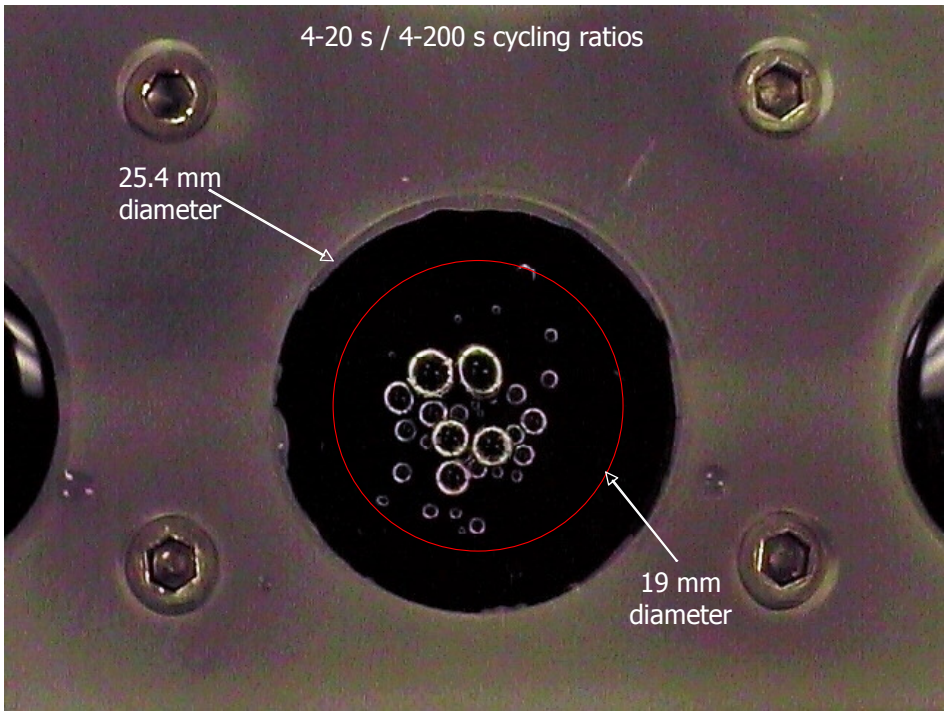

Figure 21: A characteristic bubble point test image of MEA at 90 °C.

FESEM imaging of MEA

In an effort to gain a greater understanding of the failure progression in the MEA, FESEM imaging of the as-received MEA was conducted. Typical images of the electrode cracks ("mud cracks") are shown in Fig. 22**.** In this figure, the grayish, dark regions in the images are the mud cracks present in the electrode layers of the MEA from the manufacturing process. The lighter, white regions correspond to the catalyst region. The mud cracks appear to cut all the way through the catalyst layers and terminate at the interface between the electrode layer and membrane. No membrane cracks were found under the mud cracks in the as-received samples. In Fig. 23 and Fig. 24**,** FESEM images of MEA samples tested at 90 °C under 20-20 s cycling are shown. While the as-received images show no membrane cracks present within the mud cracks, the two images of tested MEA show that there are membrane cracks within the mud cracks. These cracks show visible fibrils that are likely from the expanded polytetrafluoroethylene (e-PTFE) reinforcement layer in Gore MEA. In addition, these smaller cracks that develop within the mud cracks occur in the general location where leaking was observed to occur in bubble point testing. This observation, in conjunction with the shorter lifetimes observed for the MEA samples in comparison with the bare membrane samples, suggests that the mud cracks present in MEA act as stress concentration sites leading to cracking in the membrane itself and subsequent leaking.

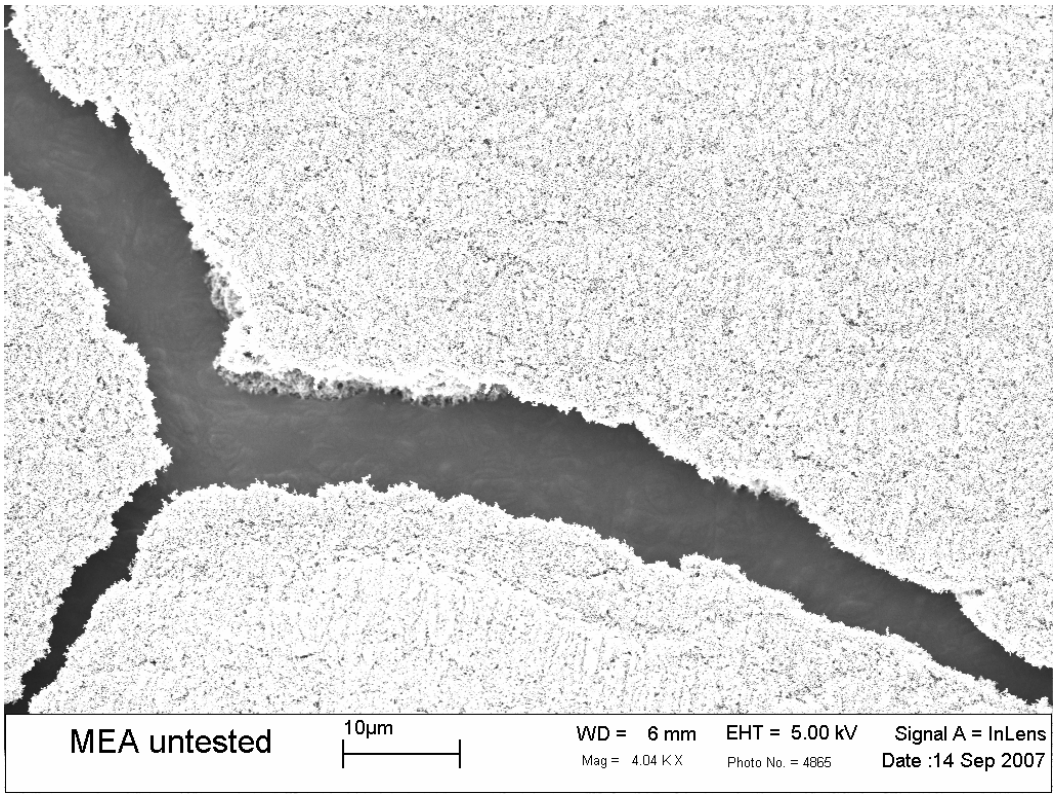

Figure 22: Image of mud crack in as-received MEA sample.

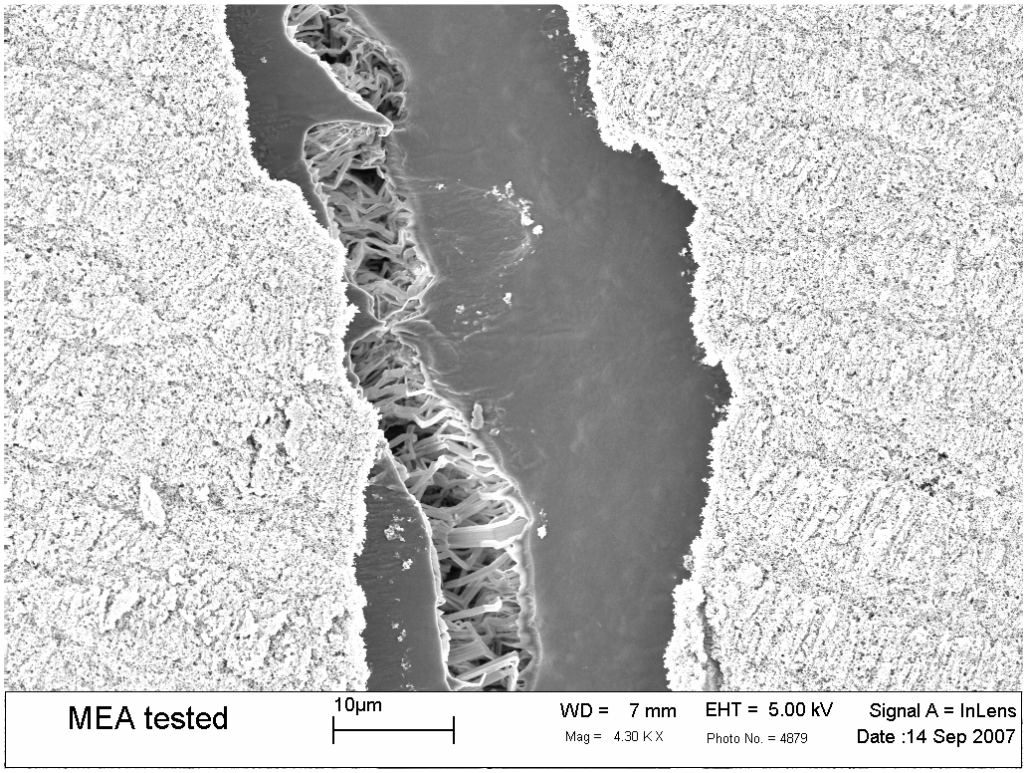

Figure 23: Image of damage within mud crack in MEA sample tested at 90 °C under 20-20 s cycling.

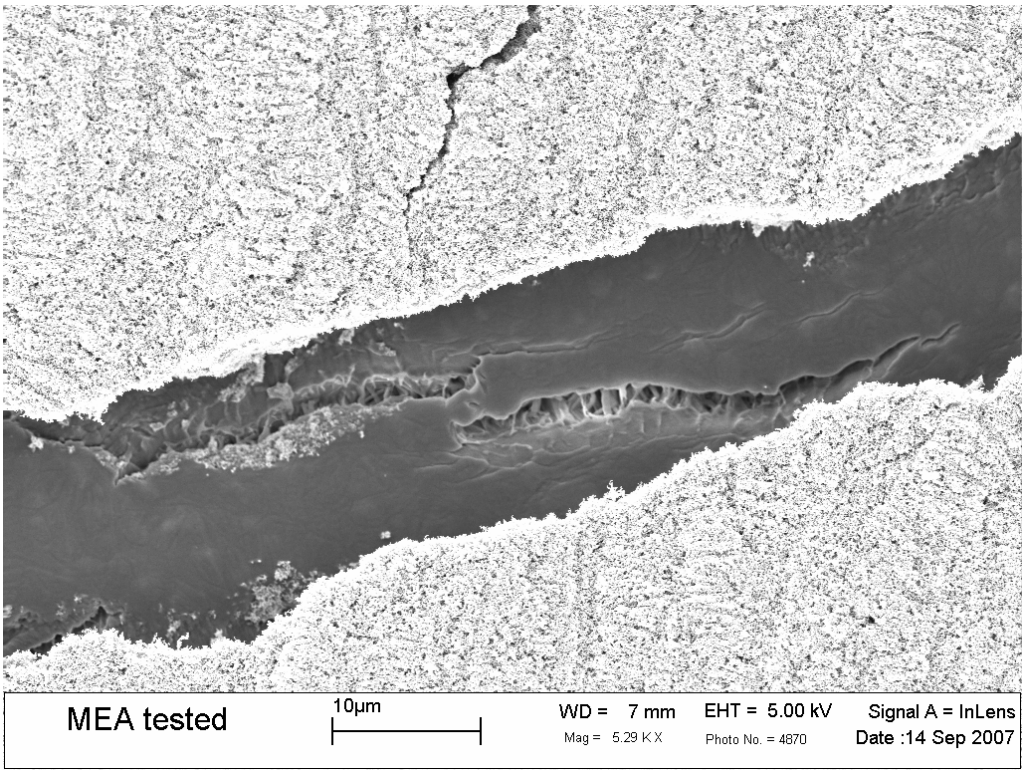

Figure 24: Image of damage within mud crack in MEA sample tested at 90 °C under 20-20 s cycling.

Discussion of results and conclusions

Biaxial fatigue tests were conducted on MEA samples using a volume-controlled blister geometry. The results from these tests indicate that MEA samples begin to leak under lower stresses than membrane samples at the same time till failure. In addition, data collected for various duty cycles indicates that the net time at load as well as the recovery period are both important factors influencing the leaking within MEA. However, the mechanisms that determine leak location relative to duty cycle are not understood at this time and need to be investigated further. The correlation with number of fatigue cycles was less evident than that of net time at load. A simple model was developed to characterize the rate of leaking during the tests. Post leaking bubble point testing was then used to identify leaking sites. FESEM imaging of the general areas around these leaking sites show that small cracks initiate within larger "mud cracks"

present in the catalyst layers of MEA. This, along with the lower stresses at failure observed for the MEA samples in comparison with the bare membranes, leads to the conclusion that the mud cracks are acting as stress concentrators that lead to premature failures. Further testing is needed to confirm these results and to determine the mechanisms and causes for leaking of MEA samples in relatively short periods of time compared to PEM samples.

Chapter 3: Fatigue Behavior of Membranes

Abstract

Mechanical fatigue testing has shown that MEAs (membrane electrode assemblies) fail at smaller stresses than PEMs (proton exchange membranes) at comparable failure times. These smaller stresses can be attributed to the presence of mud cracks in the catalyst layers acting as stress concentrators. Fatigue testing of MEAs has shown that smaller-scale cracking occurs in the membrane within these mud cracks, leading to leaking and the failure of the membrane. In addition, this testing of MEAs has further established that the cycle pattern, which affects the viscoelastic behavior of the membranes, has a significant effect on the relative lifetime of the MEA. To elucidate the viscoelastic behavior of the MEA based on these results, testing was conducted using a DMA to determine the stress relaxation behavior of the membrane. This data was then used in a FEA program (ABAQUS™) to determine its effect on the mechanical behavior of the MEA. A linear damage accumulation model used the ABAQUS™ results to predict lifetimes of the membrane in the MEAs. The models showed that under volume-controlled loading, the stress decays with time and the stress dropped towards the edges of the blisters. The lifetimes of the MEAs varied depending on the cycling pattern applied. This is important for understanding failure mechanisms of MEAs under fatigue loading, and will help the fuel cell industry in designing membranes that better withstand imposed hygrothermal stresses experienced during typical operating conditions.

Keywords: Fuel cells, membranes, mechanical behavior, fatigue lifetimes, failure, blister test, membrane electrode assembly, MEA, catalyst layer, electrode cracks, viscoelasticity, stress relaxation, DMA, FEA, ABAQUS™

Introduction

Volume controlled blister fatigue testing has shown that mud cracks introduce stress concentrations which cause MEAs to fail at lower stresses compared to bare membranes. The mechanical testing has also shown that the pressurized cycling pattern has a significant effect on the time of failure as well as the location of the failure sites within the blisters. To obtain a better understanding of these behaviors, the viscoelastic (time-dependent) behavior of the MEAs was determined using a DMA. This viscoelastic response of the MEAs was then inputted into an ABAQUS™ model to analyze stresses, strains and displacements in the membranes during mechanical fatigue testing. Using the ABAQUS™ stresses, a linear damage accumulation (LDA) model was developed to determine MEA lifetimes. Comparing these predicted LDA lifetimes with experimental results will help to develop a more complete understanding of mechanical fatigue behavior of the MEAs.

Experimental procedure – Viscoelastic testing

A TA Instruments Q800 DMA was used to run stress relaxation tests on MEA samples. The samples were cut to dimensions 5-7 mm wide by 18-22 mm long with a thickness of 0.042 mm. The testing procedure used to develop master curves under stress relaxation consisted of equilibrating at a temperature and holding for 30 minutes, undergoing loading for 3 minutes and then ramping up to the next test temperature. The test temperatures ranged from 30 to 120 °C in 10 degree intervals. All master curve tests were performed under dry air conditions using air piped in from a dry air cylindrical tank. The testing procedure used to develop long-term stress relaxation curves consisted of equilibrating at 90 °C and holding for 30 minutes and then undergoing loading for 5000

minutes. The long-term tests were performed without piping in dry air since at 90 °C the ambient air is nominally dry. Dry air conditions for testing were necessary to separate out the effects of humidity in order to focus attention solely on temperature. The dry conditions also mimic the dry air conditions in the blister fatigue tests. Also, a temperature of 90 °C was used for long-term testing and as the reference temperature for all master curves since blister fatigue testing was conducted at this temperature. The viscoelastic information obtained from the DMA will be used for modeling.

Dynamic Mechanical Analysis

In Fig. 25, both time-temperature super-position (TTSP) stress relaxation master curves and long term stress relaxation curves are plotted. The long term curves differ from the TTSP curves only at long times where the long term curves appear to reach a plateau. The two low modulus TTSP curves have gaps in them due to sudden and unexpected drops in modulus at 100 °C and 110 °C. These modulus drops are represented in the shift factor plots shown in Fig.26. These stress relaxation curves are being used to describe the material properties of Gore MEAs in a model, including the model described later in this chapter.

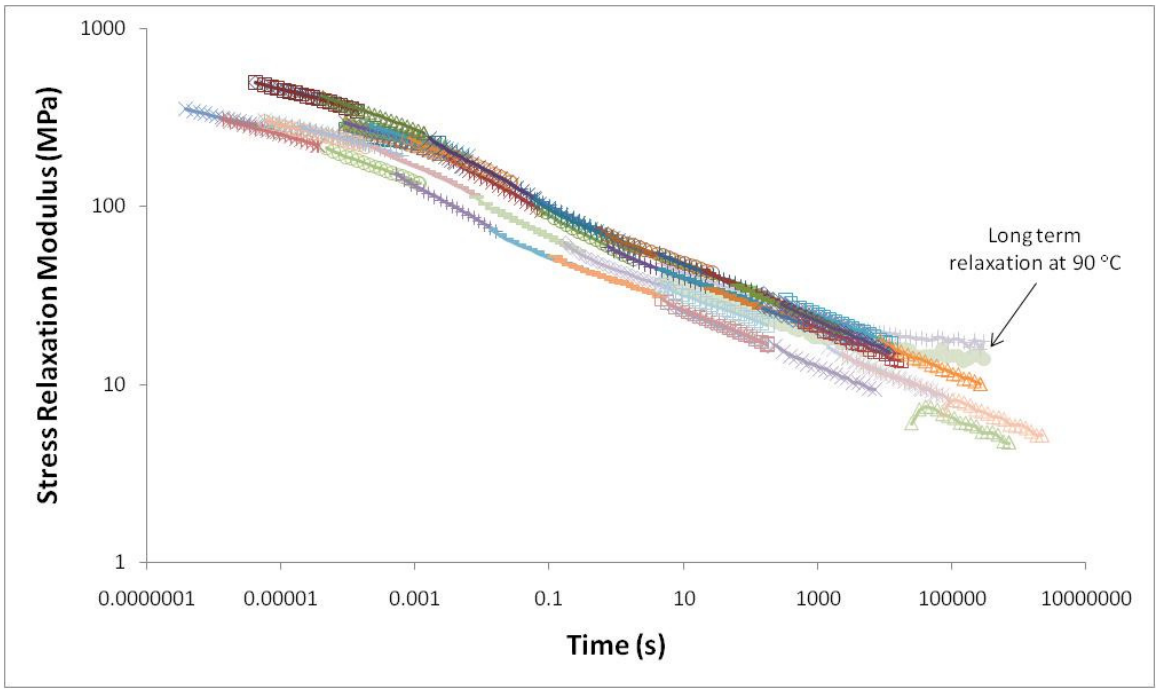

Figure 25: Five TTSP stress relaxation master curves and two long term stress relaxation curves all from seven different samples of Gore MEA referenced at 90 °C under dry conditions.

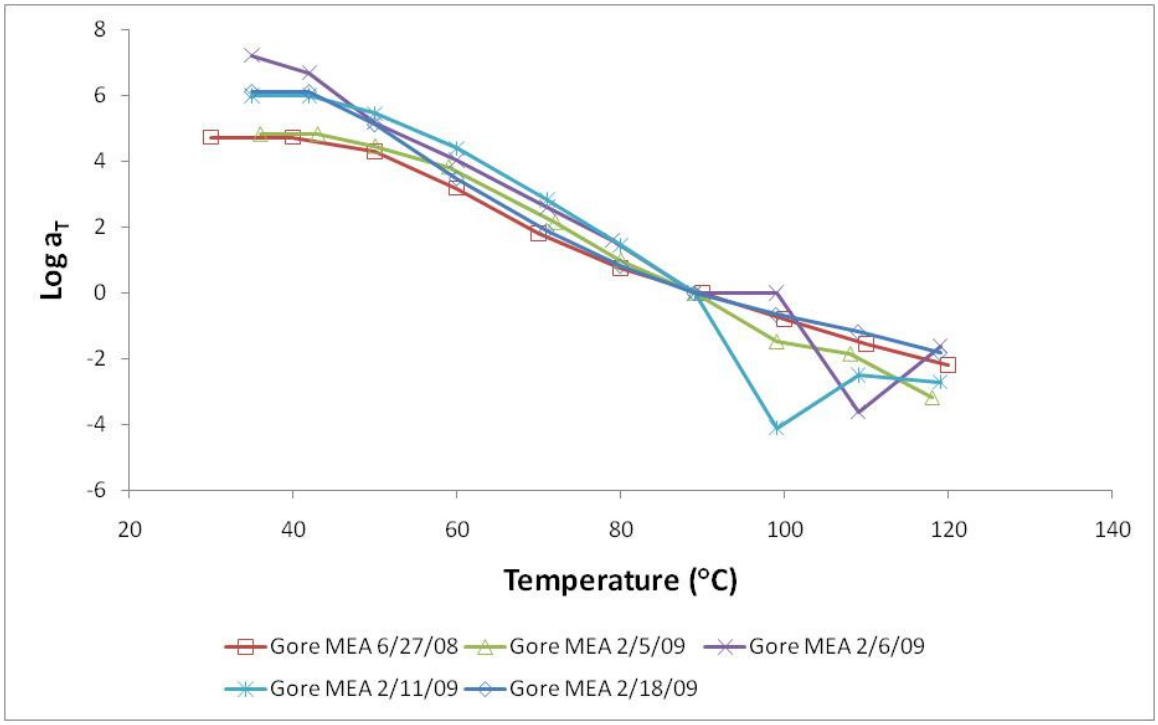

Figure 26: Shift factor plots for the TTSP stress relaxation master curves of Gore MEA from Fig. 25.

ABAQUS™ modeling and linear damage accumulation analysis

An analytical model was developed to calculate the expected volumes and pressures generated during blister fatigue testing. A schematic of this approach is shown in Fig. 27. The ideal gas law was applied in order to calculate the pressures and volumes. Four equations were used to calculate the volumes in the blister chambers. The volume of the blister as a function of pressure was estimated using the Hencky solution for the displacement of a blister to solve for volume as in eqn. (1). This results in the expression in eqn. (2). In eqn. (2), 'a' is the radius of the blister; 'p' is the pressure; 'E' is Young's modulus and 'h' is the blister thickness. The volume-controlled blister fixture contains tubing that connects the block itself to pressure sensors for each of the chambers. Thus, a volume for these lines is needed and is estimated in eqn. (3) using the radii and lengths of the different sized tubing composing these lines. The volume in each of the chambers, represented by eqn. (4), is calculated based on the volume of a cylinder. The overall volume [eqn. (5)] is the summation of the three previously described volumes where V_{line} is constant, $V_{chamber}$ drops when the piston is raised during testing and $V_{blister}$ changes over time during testing depending on the pressures applied.

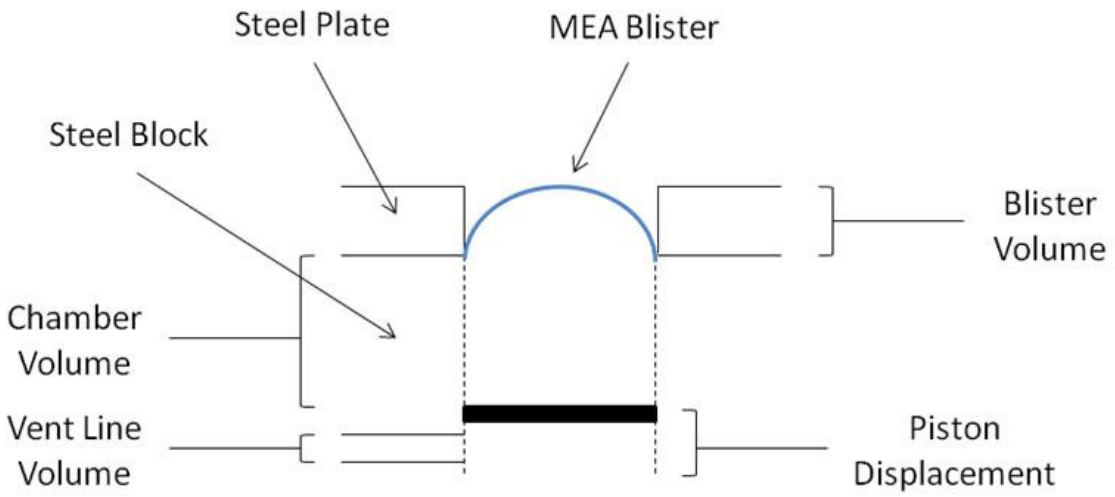

Figure 27: Schematic of analytical model of blister volumes and pressures.

$$V = \int_0^a \left(2\pi \times r \times u\left(r/a\right)\right) dr \tag{1}$$

$$V_{blister} = 1.021 a^3 \left(\frac{ap}{Eh}\right)^{1/3} \tag{2}$$

$$V_{line} = length_{small\_tube} \pi r_{small\_tube}^{\ 2} + length_{thick\_tube} \pi r_{thick\_tube}^{\ 2} \tag{3}$$

$$V_{chamber} = height_{chamber} \pi r_{chamber}^{\ 2} \tag{4}$$

$$V_{overall} = V_{chamber} + V_{blister} + V_{line} \tag{5}$$

The results of this analytical model are shown in Table 2 for the largest and smallest piston displacements (7.541 mm and 5.159 mm). The resulting analytical pressures are represented by P_{anal} while the pressures seen experimentally are represented by P_{exp}.

Table 2: Analytical results based on piston displacements in volume-controlled blister fixture.

	$V_{chamber}$ (m^3)	$V_{blister}$ (m^3)	$V_{overall}$ (m^3)	P_{anal} (kPa)	P_{exp} (kPa)
7.54 mm	8.53E-06	4.04E-07	8.94E-06	19.79	19
5.16 mm	9.21E-06	3.42E-07	9.55E-06	11.97	13

A model was developed in ABAQUS™ to analyze the stresses, strains and displacements of blisters of Gore MEAs based on a constant-volume pressurization of these blisters over time [38, 40, 43, 44]. The constant volume was obtained using a piston element traveling a prescribed distance (a specified amplitude displacement in the

ABAQUS™ model) thus pressurizing the constrained blisters using a constant volume of air from underneath. This is similar to the way the volume-controlled blister fixture operates. The MEA blister was separated into three layers, catalyst-membrane-catalyst, where each layer has several nodes from the center towards the edge of the blisters where the stresses, strains and displacements were analyzed. There were 2000 nodes for each of these three layers from the center to the edge. All 6000 of the elements associated with these nodes were axisymmetric shells, SAX1. The nodes in each of the three layers were tied together such that the displacements in the radial and thickness directions were the same for each layer. The bulk modulus was assumed to be independent of time and ν_0 = 0.4 for each material. Poisson's ratio, ν, was allowed to change with time consistent with a constant bulk modulus. Non-linear geometric analysis was conducted. The catalyst layers were 12 μm thick while the inner membrane layer was 18 μm thick. The ABAQUS™ model was symmetric with each layer having a 9.525 mm radius. The loading was cycled under various patterns for 20 full cycles. The cycling patterns of time under load vs. time under recovery were 4-200, 4-20, 4-4, 20-20, 100-100, 20-4 and 200-4. The displacements used to pressurize the MEAs were selected based on the total chamber volume in the ABAQUS™ model matching the total chamber volume plus the volume in the pressure sensor lines present in the volume-controlled blister experiments as described above. The material properties of each layer of the MEA are defined by the long term stress relaxation curves described earlier, including deriving the catalyst layer properties based on MEA and PEM long term stress relaxation curves. These long term stress relaxation curves are shown in Fig. 28. The resulting ABAQUS™ stresses for a 4-4 s fatigue test are shown in Fig. 29 – Fig. 32. The in-plane principal catalyst layer

stresses for the loading portion of the fatigue cycle are shown in Fig. 29 while, the stresses during the recovery portion of the fatigue cycle are shown in Fig. 30. The in-plane principal membrane stresses for the loading portion of the fatigue cycle are shown in Fig. 31 while, the stresses during the recovery portion of the fatigue cycle are shown in Fig. 32. The stresses in the catalyst layers are shown to be higher than those in the membrane. While stresses in the catalyst layers are higher near the edges of the blister during recovery, the magnitude of the stresses during loading are higher by more than a factor of ten in the center of the blister. The stresses in the membrane tend to be compressive during recovery and in tension during loading. Figure 29 – Figure 32 also show that the stresses drop in magnitude during each fatigue cycle. These resulting stresses in the membrane and catalyst layers were then used in a linear damage accumulation model (LDA) to calculate the lifetimes of the MEA assuming no cracks formed in the catalyst layers.

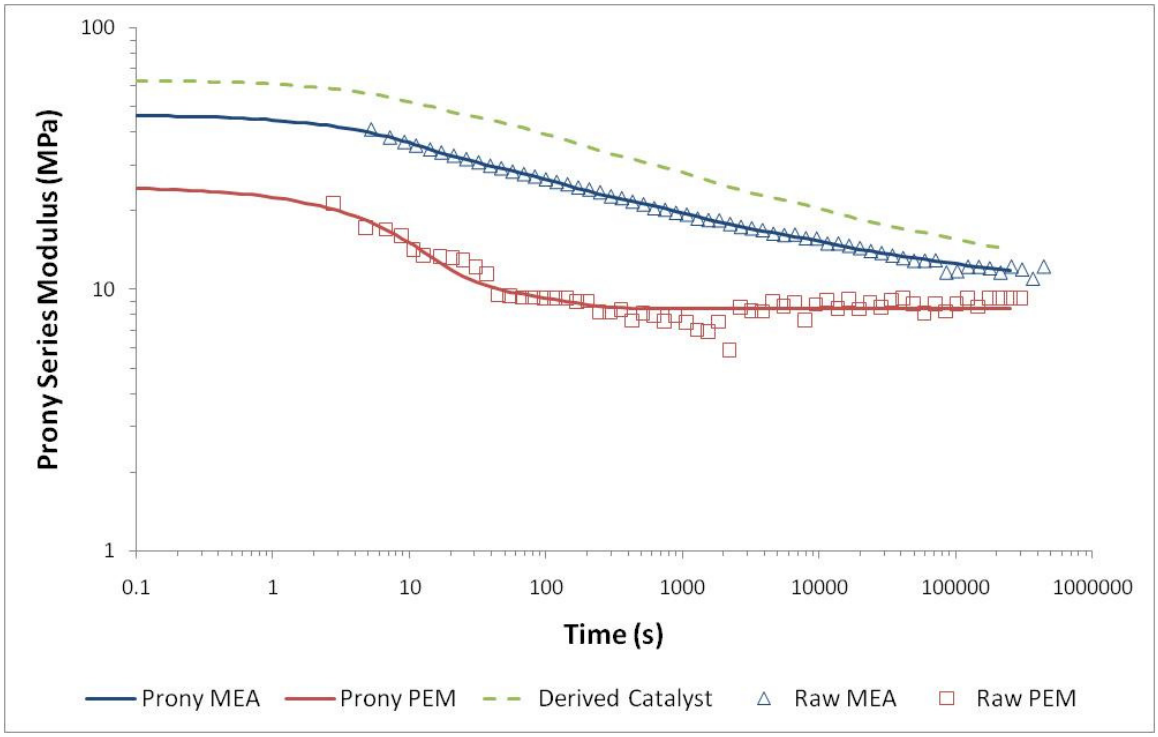

Figure 28: Prony series curves used in ABAQUS™ model.

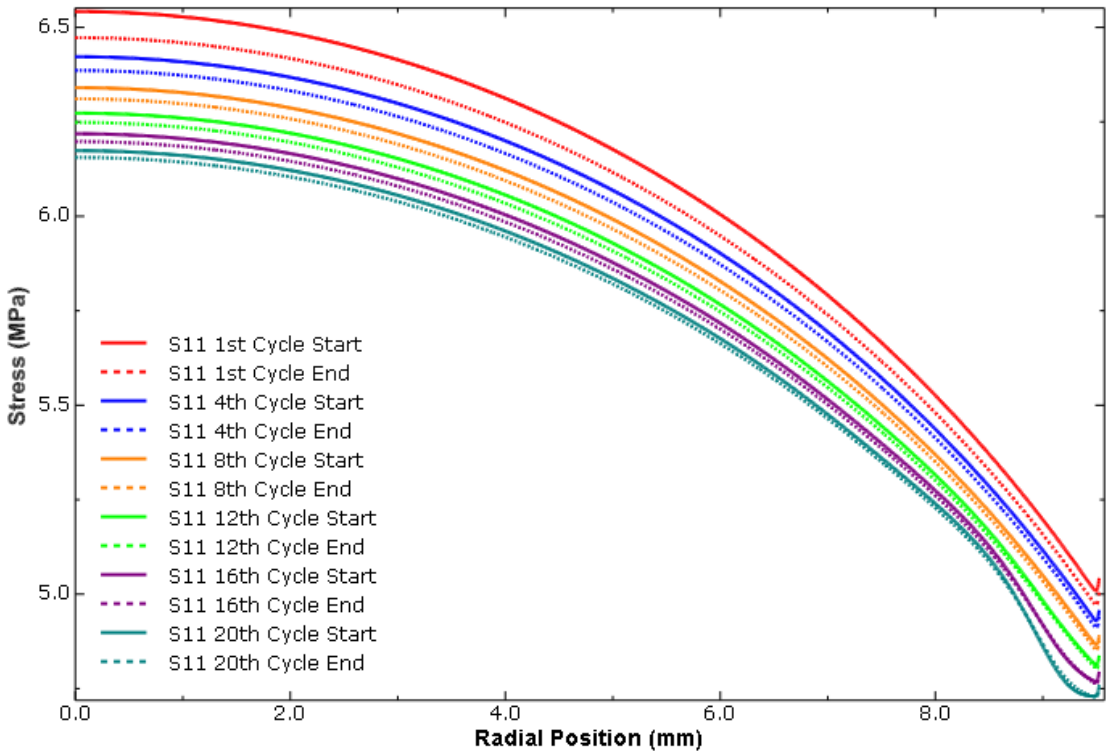

Figure 29: ABAQUS™ σ_{11} for catalyst layers during 4 s loading periods.

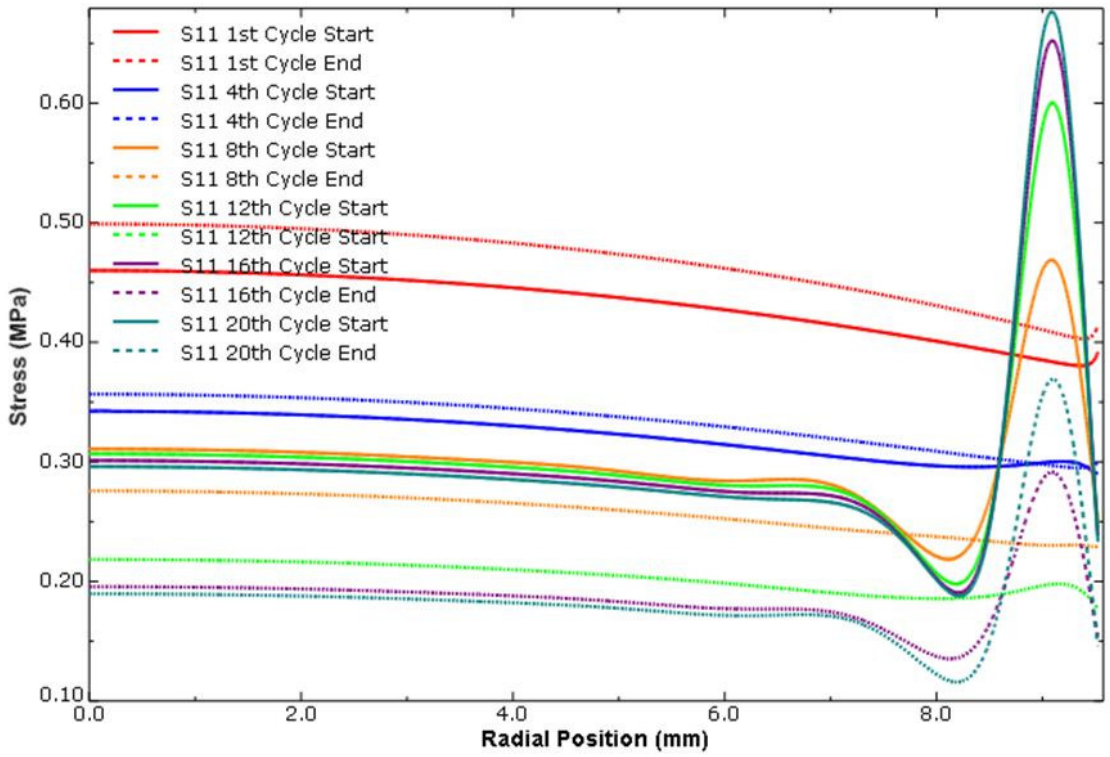

Figure 30: ABAQUS™ σ_{11} for catalyst layers during 4 s recovery periods.

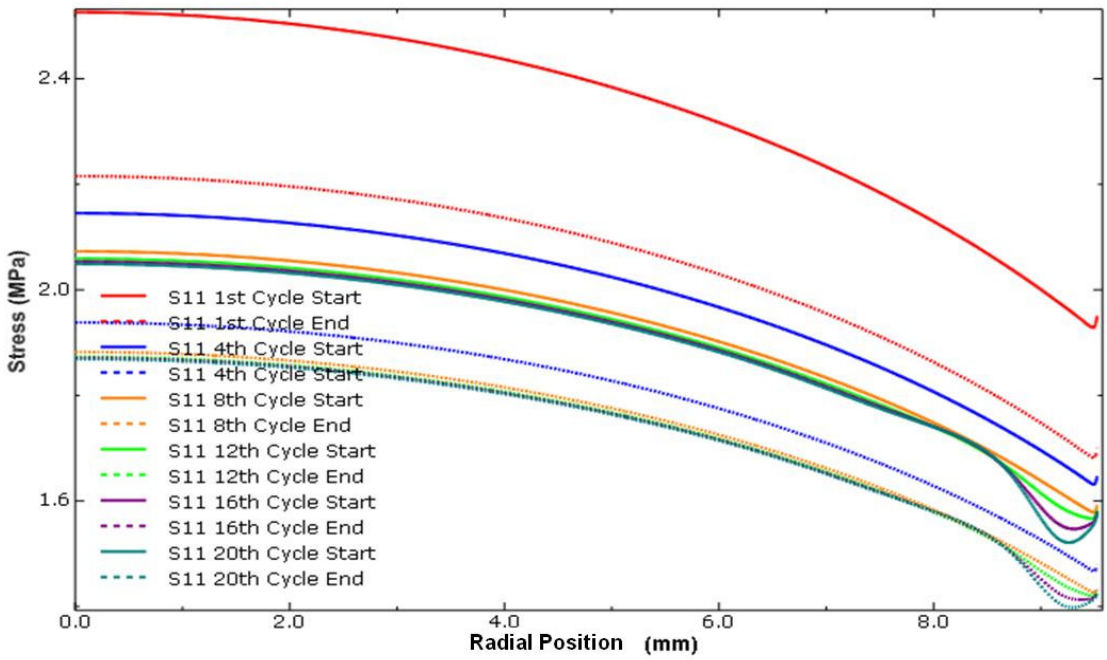

Figure 31: ABAQUS™ σ_{11} for membrane during 4 s loading periods.

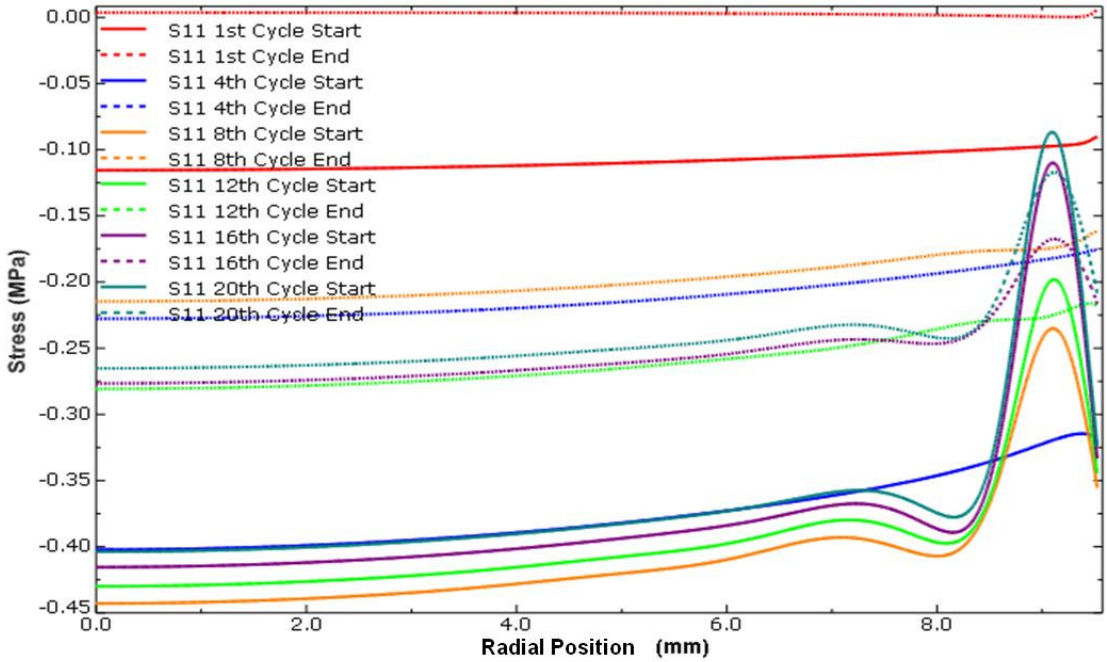

Figure 32: ABAQUS™ σ_{11} for membrane during 4 s recovery periods.

In this LDA model, we assume that failure occurs as a result of the accumulation of damage during the time spent at a particular stress level. To implement the model, we calculate the damage that develops during a single cycle as eqn. (6)

$$D = \int \frac{dt}{\tau} \tag{6}$$

where the time-to-failure as a function of the current stress level is estimated as eqn. (7) [38].

$$\tau = A\sigma^{B} = 4960000\sigma^{-4.69} \tag{7}$$

The accumulated damage is then summed over each cycle until failure is predicted to occur (when the total damage is equal to unity). In practice, the stress analysis is performed for the first twenty cycles, and then it is assumed that the stresses for all subsequent cycles are equal to those for the twentieth cycle. The resulting damage accumulation expression is eqn. (8).

$$\Sigma_1 \frac{\Delta t}{\tau} + \Sigma_2 \frac{\Delta t}{\tau} + \ldots + (N-19)\Sigma_{20} \frac{\Delta t}{\tau} = 1 \tag{8}$$

Equation (8) is then solved for the number of cycles to failure, *N*.

Predictions developed using this model as well as the experimental data for 7.541 mm, 6.746 mm, 5.953 mm and 5.159 mm piston displacements are shown in Fig. 33 and Fig. 34. Figure 33 represents lifetime in terms of the number of cycles until failure while Fig. 34 represents lifetime in terms of the net time under load until failure. In Fig. 33 and Fig. 34, the predicted lifetimes are plotted versus the experimental lifetimes, so that predictions perfectly in agreement with the data would fall along the line of perfect agreement. In Fig. 33 and Fig. 34, we see that the predicted lifetimes are much greater than the experimental lifetimes. This finding is not surprising given the presence of the cracks in the catalyst layers. The challenge, of course, is to develop a reasonable means to incorporate these cracks into the lifetime prediction analysis. As a first engineering estimate, an effective stress is calculated using the force resultants involving stresses in

both the membrane and catalyst layers and then discounting the catalyst layers by dividing by the membrane layer thickness as shown in eqn. (9).

$$\tilde{\sigma} = \sigma^m + 2\sigma^c \frac{t^c}{t^m} \tag{9}$$

In eqn. (9), m refers to the membrane layer while c refers to the catalyst layers. This effective stress is then used in the LDA analysis. This modified stress assumes that there are large mud cracks throughout the catalyst layers thus entirely discounting the catalyst layers' ability to bear any of the loads within the MEA. Lifetimes calculated in this fashion are shown in Fig. 35 and Fig. 36. In these figures, the data points are consistently well below the perfect agreement line. This suggests that the LDA analysis using the effective stresses over predicts the effects of mud cracks, or damage in the catalyst layers. It also suggests that the actual state of the MEAs lies somewhere in-between these two extreme cases.

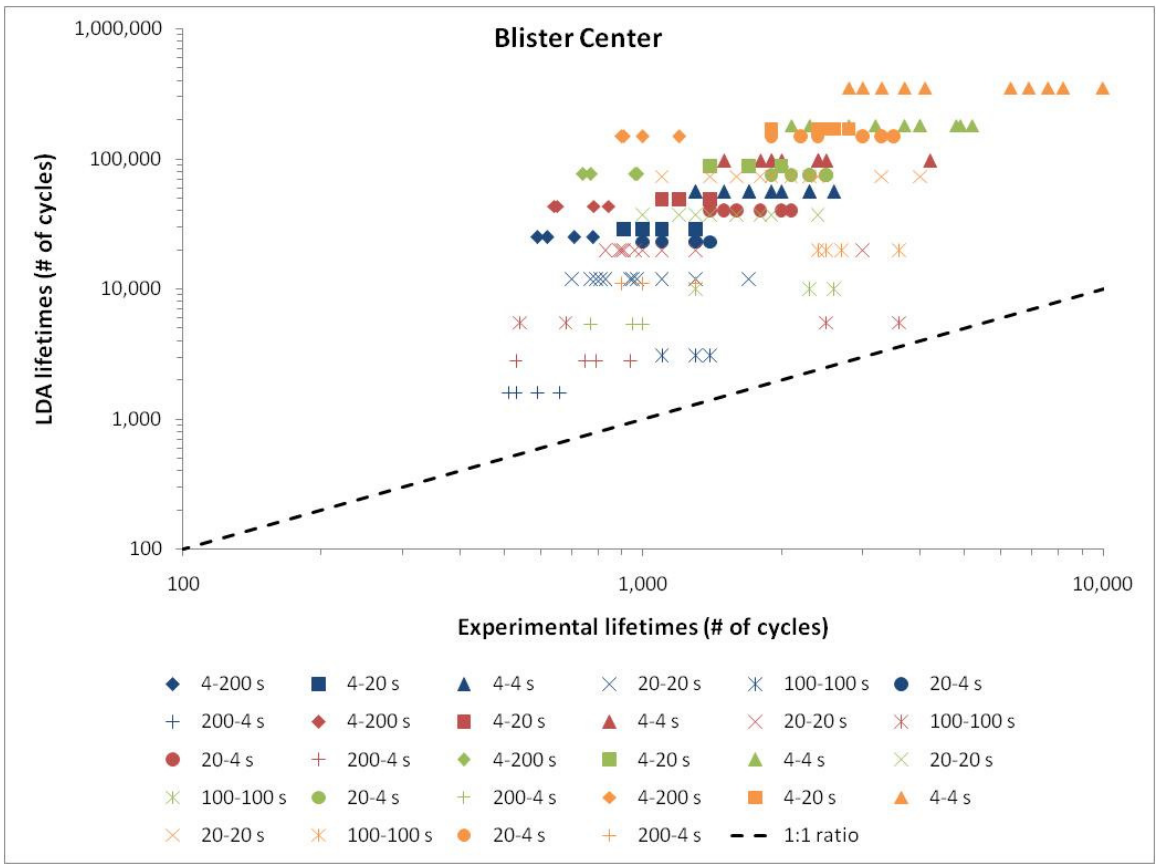

Figure 33: LDA vs. experimental lifetime results based on membrane ABAQUS™ stresses with no degradation in catalyst layers.

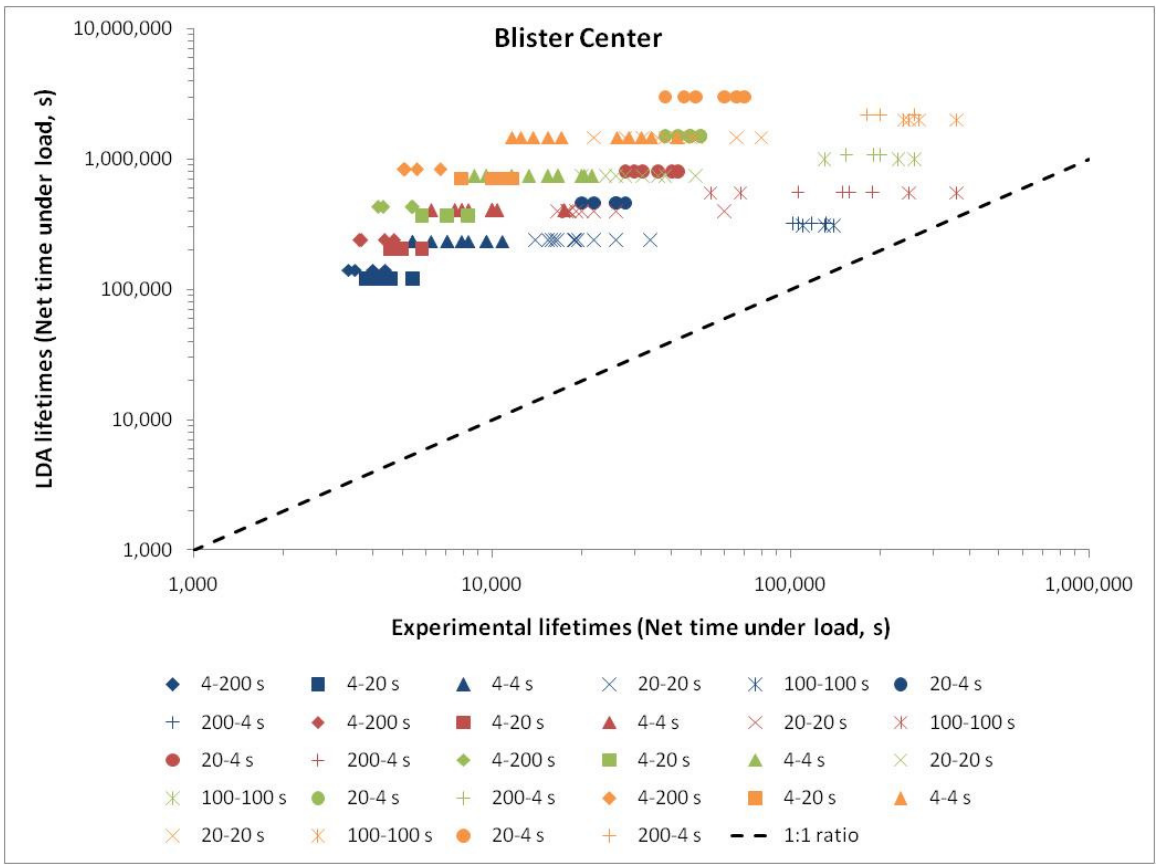

Figure 34: LDA vs. experimental lifetime results based on membrane ABAQUS™ stresses with no degradation in catalyst layers.

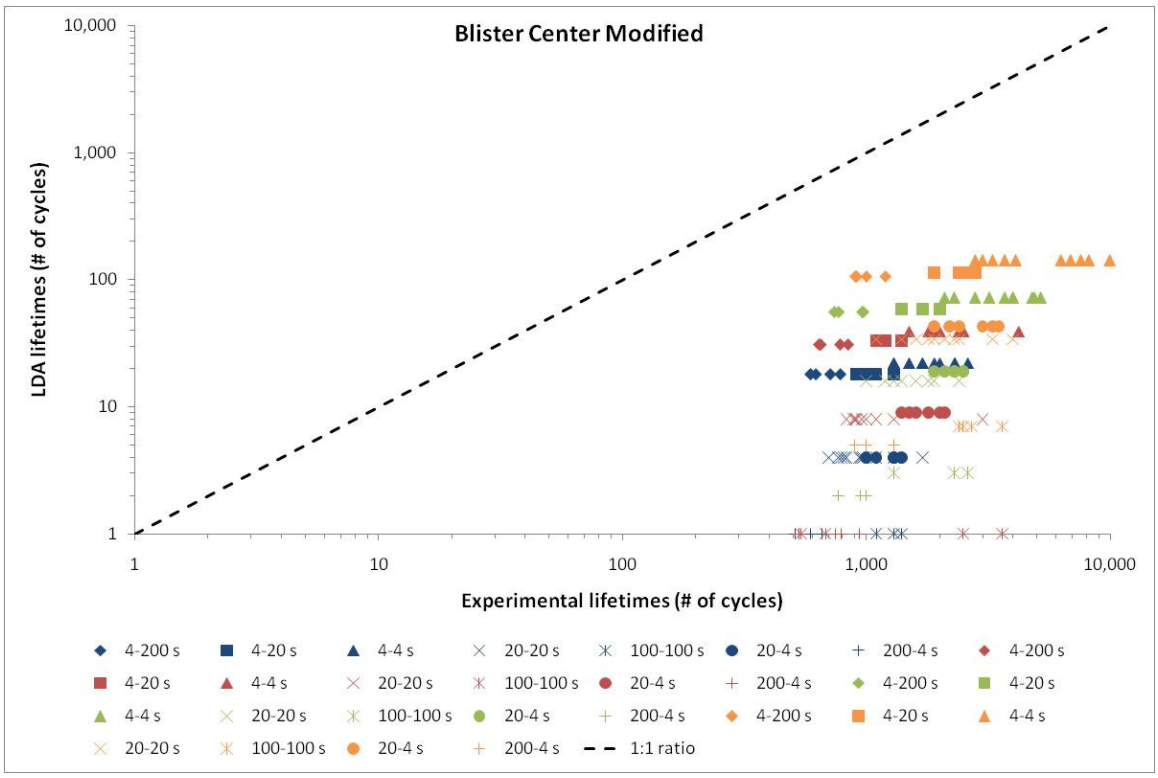

Figure 35: LDA vs. experimental lifetime results based on both membrane and catalyst layer ABAQUS™ stresses and discounting the catalyst layers during analysis.

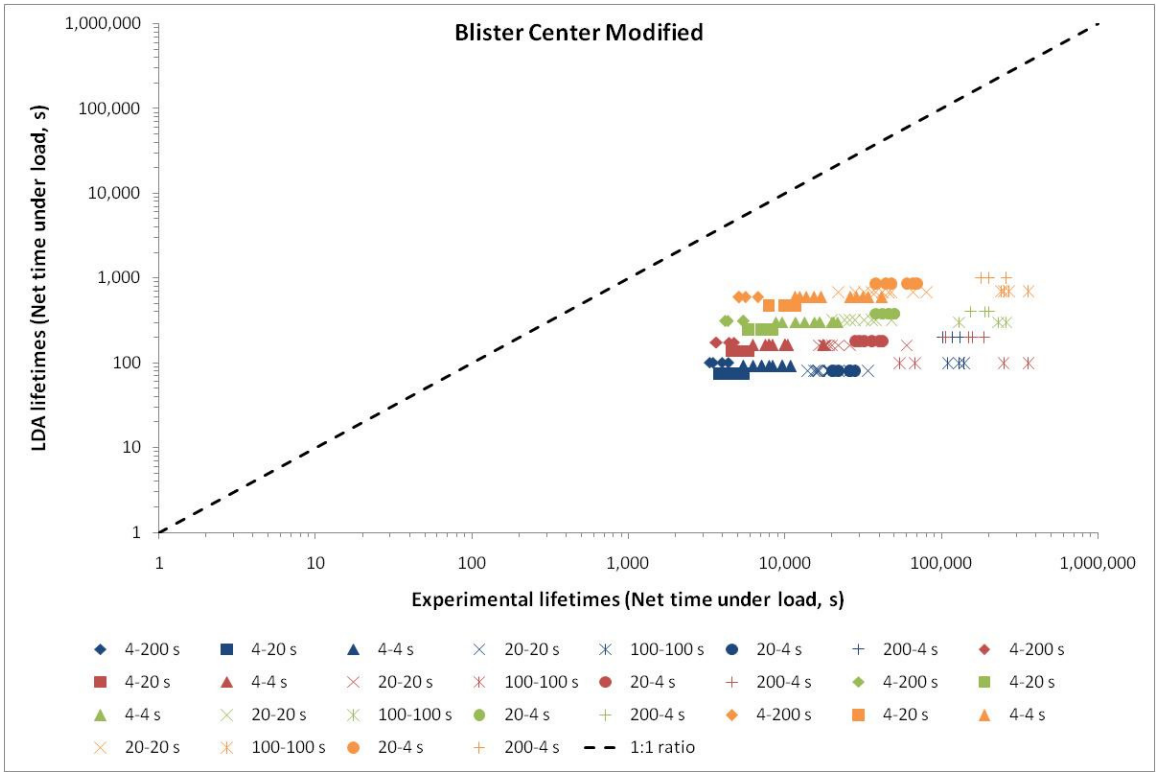

Figure 36: LDA vs. experimental lifetime results based on both membrane and catalyst layer ABAQUS™ stresses and discounting the catalyst layers during analysis.

Discussion of results and conclusions

The ABAQUS™ stress analysis based on the membrane stresses did not match up well with experimental work. This mismatch that was caused by an assumption of no cracks in the catalyst layers resulted in model lifetimes significantly off experimentally determined lifetimes. This means that a more accurate prediction of lifetimes that incorporates mud cracks in the catalyst layers and the resulting stress / strain concentrations was needed. An engineering estimate was used to determine an effective stress to input into the LDA model. This engineering estimate assumed that large mud cracks existed throughout the membrane thus effectively discounting the catalyst layers' ability to bear any load. The MEAs in actuality have mud cracks present in the catalyst layers before testing and fail in the localized regions within these mud cracks. The MEA catalyst layers also are able to bear load due to the relative low density of mud cracks present in the as-received state. This means that a more accurate prediction of lifetimes that better incorporates the true presence of mud cracks within the catalyst layers and the resulting stress / strain concentrations is needed. The models do show that the lifetimes of Gore MEA vary depending on the cycling pattern applied similar to what the experimental results have shown.

Chapter 4: Overall Conclusions

Summary of results and their implications

Volume-controlled blister fixture testing has shown that MEA samples fail at smaller stresses than PEM samples under the same times till failure. The cycling pattern or duty cycle has a significant effect on the fatigue lifetimes of Gore MEAs. MEA samples under 4-200 s and 4-20 s cycling fail first followed by 4-4 s and 20-20 s cycled samples and then 20-4 s, 100-100 s and 200-4 s cycled samples. Failure sites also tended to vary based upon the duty cycle. MEA samples that underwent short loading relative to recovery failed at the center of the blisters. MEA samples that underwent long loading relative to recovery failed near the edges of the blisters. MEA samples that underwent equal loading and recovery tended to fail both at the center and near the edges of the blisters. SEM images have shown that ionomer cracks exist within catalyst layer mud cracks in these regions. This suggests that the catalyst layer mud cracks have a significant effect on the lifetimes of MEAs and that the duty cycle affects where and when failures occur within the membranes.

Viscoelastic tests were conducted to determine the time-dependent nature of the mechanical behavior of MEAs. The viscoelastic data was used to conduct ABAQUS™ stress analysis on the MEAs three-layered structure of catalyst-membrane-catalyst. These ABAQUS™ stresses were then inputted into a LDA model to determine MEA lifetimes and compare them to experimentally determined lifetimes. The results showed that LDA lifetimes based on ABAQUS™ stresses, calculated assuming no catalyst layer defects, tended to be far longer than MEA lifetimes seen experimentally. This is inaccurate due to the fact that catalyst layers contain several mud cracks in their as-

received state. An engineering estimate was conducted where an effective stress was calculated and inputted into the LDA analysis. This assumed large mud cracks existed throughout the catalyst layers effectively discounting their ability to bear load within the MEAs. This resulted in the LDA analysis predicting lifetimes much shorter than MEA lifetimes seen experimentally. Thus, a more accurate LDA analysis is needed to better represent the true state of MEAs and predict more accurate MEA lifetimes. Unfortunately, the LDA analysis with ABAQUS™ stresses also does not shine any further light on why the failure sites change depending on the duty cycle.

Future direction of subsequent research

Further research is needed to determine the cause of some key observations. The reason beyond the migration of leak sites due to different duty cycles is not clearly understood. ABAQUS™ stress analysis has shown higher stresses near the edges of the blister during recovery. However, there magnitudes are not significantly higher than stresses in the center of the blister during loading to contribute to failures near the edge. Further stress analysis work is needed to examine the stresses (and possibly strains) throughout MEA blisters during loading. The LDA analysis can be improved using such techniques as including stress concentrations due to catalyst layer mud cracks and including both the stress history based on the number of cycles and the stress history based on test times in determining lifetimes. Thus, both lifetimes based on cycling as well as the net time under load were shown in the LDA vs. experimental lifetime plots (Fig. 33 - Fig. 36). These show that the best agreement between LDA lifetimes and experimental lifetimes might exist as a combination of the number of cycles and net time under load results. These figures also show that while the catalyst layers are not

completely free of defects, they do not contain so many mud cracks that the load-bearing capability of the catalyst layers can be completely dismissed. Another avenue that needs to be pursued is to examine how duty cycles are affecting PEM lifetimes by testing PEM samples using the volume-controlled blister fixture under 4-200 s, 4-20 s, 4-4 s, 20-20 s, 100-100 s, 20-4 s and 200-4 s cycling. This will help determine if the duty cycle effects the location of failure as well as the lifetime duration of PEM samples similarly to that of MEA samples under the same test conditions.

References

1. Nancy L. Garland, J.P.K., *The United States Department of Energy's high temperature, low relative humidity membrane program.* Journal of Power Sources, 2007. **172**: p. 94-99.
2. Rod Borup, J.M., Brya Pivovar, Yu Seung Kim, Rangachary Mukundan, Nancy Garland, Deborah Myers, Mahlon Wilson, Fernando Garzon, David Wood, Piotr Zelenay, Karren More, Ken stroh, Tom Zawodzinski, James Boncella, James E. McGrath, Minoru Inaba, Kenji Miyatake, Michio Hori, Kinichiro Ota, Zempachi Ogumi, Seizo Miyata, Atsushi Nishikata, Zyun Siroma, Yoshiharu Uchimoto, Kazuaki Yasuda, Ken-ichi Kimijima, Norio Iwashita, *Scientific Aspects of Polymer Electrolyte Fuel Cell Durability and Degradation.* American Chemical Society, Chemical Reviews, 2007: p. 3904-3951.
3. Uwe Benscher, S.J.C.C., William B. Johnson, *Challenges for PEM fuel cell membranes.* International Journal of Energy Research, 2005. **29**: p. 1103-1112.
4. M. A. Hickner, B.S.P., *The Chemical and Structural Nature of Proton Exchange Membrane Fuel Cell Properties*, in *Fuel Cells*. 2005, WILEY-VCH Verlag GmbH & Co. KGaA: Weinheim. p. 213-229.
5. Michael A. Hickner, H.G., Yu Seung Kim, Brian R. Einsla, James E. McGrath, *Alternative Polymer Systems for Proton Exchange Membranes (PEMs).* American Chemical Society, Chemical Reviews, 2004. **104**: p. 4587-4612.
6. Yanxiang Li, A.R., Anand S. Badami, Melinda Hill, Juan Yang, Stuart Dunn, James E. McGrath, *Synthesis and characterization of partially fluorinated hydrophobic-hydrophilic multiblock copolymers containing sulfonate groups for proton exchange membrane.* Journal of Power Sources, 2007. **172**: p. 30-38.
7. Yu Seung Kim, F.W., Michael Hickner, Stephen McCartney, Young Taik Hong, William Harrison, Thomas A. Zawodzinski, James E. McGrath, *Effect of Acidification Treatment and Morphological Stability of Sulfonated Poly(arylene ether sulfone) Copolymer Proton-Exchange Membranes for Fuel-Cell Use above 100 °C.* Journal of Polymer Science: Part B: Polymer Physics, 2003. **41**: p. 2816-2828.

8. T. R. Ralph, D.E.B., P. J. Bouwman, A. J. Hodgkinson, M. I. Petch, M. Pollington, *Reinforced Membrane Durability in Proton Exchange Membrane Fuel Cell Stacks for Automotive Applications.* Journal of Electrochemical Society, 2008. **155**(4): p. B411-B422.
9. Yaliang Tang, A.K., Anette M. Karlsson, Michael H. Santare, Simon Cleghorn, William B. Johnson, *Mechanical properties of a reinforced composite polymer electrolyte membrane and its simulated performance in PEM fuel cells.* Journal of Power Sources, 2007. **175**: p. 817-825.
10. M. Prasanna, E.A.C., T.-H. Lim, I.-H. Oh, *Effects of MEA fabrication method on durability of polymer electrolyte membrane fuel cells.* Electrochimica Acta, 2008. **53**: p. 5434-5441.
11. Wu Bi, T.F.F., *Temperature Effects on PEM Fuel Cell Pt/C Catalyst Degradation.* Journal of the Electrochemical Society, 2008. **155**(2): p. B215-B221.
12. Yuyan Shao, G.Y., Zhenbo Wang, Yunzhi Gao, *Proton exchange membrane fuel cell from low temperature to high temperature: Material challenges.* Journal of Power Sources, 2007. **167**: p. 235-242.
13. W. Grellmann, S.S., *Deformation and Fracture Behaviour of Polymers*. 2001, Berlin: Springer.
14. Rod L. Borup, J.R.D., Fernando H. Sarzon, David L. Wood, Michael A. Inbody, *PEM fuel cell electrocatalyst durability measurements.* Journal of Power Sources, 2006. **163**: p. 76-81.
15. Vesna Stanic, M.H. *Proton Conducting Membrane Fuel Cells IV*. in *The Electrochemical Society Proceedings Series*. 2004. Pennington, New Jersey.
16. Z. X. Liang, T.S.Z., C. Xu, J. B. Xu, *Mircoscopic characterizations of membrane electrode assemblies, prepared under different hot-pressing conditions.* Electrochimica Acta, 2007. **53**: p. 894-902.
17. Ahmet Kusoglu, A.M.K., Michael H. Santare, Simon Cleghorn, William B. Johnson, *Mechanical response of fuel cell membranes subject to a hygro-thermal cycle.* Journal of Power Sources, 2006. **161**: p. 987-996.
18. Yaliang Tang, M.H.S., Anette M. Karlsson, Simon Cleghorn, William B. Johnson, *Stresses in Proton Exchange Membranes Due to Hygro-Thermal Loading.* Journal of Fuel Cell Science and Technology, 2006. **3**: p. 119-124.
19. Matt Crum, W.L., *Effective Testing Matrix for Studying Membrane Durability in PEM Fuel Cells: Part 2. Mechanical Durability and Combined Mechanical and Chemical Durability.* ECS Transactions, 2006. **3**(1): p. 541-550.
20. Xinyu Huang, R.S., Yue Zou, Matthew Feshler, Kenneth Reifsnider, David Condit, Sergei Burlatsky, Thomas Madden, *Mechanical Endurance of Polymer Electrolyte Membrane and PEM Fuel Cell Durability.* Journal of Polymer Science, Part B, Polymer Physics, 2006. **44**: p. 2346-2357.
21. Feng Rong, C.H., Zhong-Sheng Liu, Datong Song, Qianpu Wang, *Microstructure changes in the catalyst layers of PEM fuel cells induced by load cycling Part I: Mechanical model.* Journal of Power Sources, 2008. **175**: p. 699-711.
22. Feng Rong, C.H., Zhong-Sheng Liu, Datong Song, Qianpu Wang, *Microstructure changes in the catalyst layers of PEM fuel cells induced by load cycling Part II: Simulation and understanding.* Journal of Power Sources, 2008. **175**: p. 712-723.

23. Nagappan Ramaswamy, N.H., Sanjeev Mukerjee, *Degradation mechanism study of perfluorinated proton exchange membrane under fuel cell operating conditions.* Electrochimica Acta, 2008. **53**: p. 3279-3295.
24. Fang Wang, H.T., Mu Pan, Daoxi, *Ex situ investigation of the proton exchange membrane chemical decomposition.* International Journal of Hydrogen Energy, 2008. **33**: p. 2283-2288.
25. Wen Liu, M.C., *Effective Testing Matrix for Studying Membrane Durability in PEM Fuel Cells: Part I. Chemical Durability.* ECS Transactions, 2006. **3**(1): p. 531-540.
26. D. Liu, S.C., *Durability study of proton exchange membrane fuel cells under dynamic testing conditions with cyclic current profile.* Journal of Power Sources, 2006. **162**: p. 521-531.
27. Ahmet Kusoglu, A.M.K., Michael H. Santare, Simon Cleghorn, William B. Johnson, *Mechanical behavior of fuel cell membranes under humidity cycles and effect of swelling anisotropy on the fatigue stresses.* Journal of Power Sources, 2007. **170**: p. 345-358.
28. Haolin Tang, S.P., San Ping Jiang, Fang Wang, Mei Pan, *A degradation study of Nafion proton exchange membrane of PEM fuel cells.* Journal of Power Sources, 2007. **170**: p. 85-92.
29. Roham Solasi, Y.Z., Xinyu Huang, Kenneth Reifsnider, David Condit, *On mechanical behavior and in-plane modeling of constrained PEM fuel cell membranes subjected to hydration and temperature.* Journal of Power Sources, 2007. **167**: p. 366-377.
30. S. Kundu, M.w.F., L. C. Simon, S. Grot, *Morphological features (defects) in fuel cell membrane electrode assemblies.* Journal of Power Sources, 2006. **157**: p. 650-656.
31. J. Andersons, Y.L., *Advanced fragmentation stage of oxide coating on polymer substrate under biaxial tension.* Thin Solid Films, 2005. **471**: p. 209-217.
32. N. E. Jansson, Y.L., J. A. E. Månson, *Modeling of multiple cracking & decohesion of a thin film on a polymer substrate.* Engineering Fracture Mechanisms, 2006. **73**: p. 2614-2626.
33. Roulin-Moloney, A.C., *Fractography and Failure Mechanisms of Polymers and Composites*. 1989, New York: Elsevier Applied Science.
34. Schiers, J., *Compositional and Failure Analysis of Polymers: A Practical Approach*. 2000, Chichester: John Wiley & Sons.
35. Yongqiang Li, J.K.Q., Scott W. Case, Michael W. Ellis, David A. Dillard, Yeh-Hung Lai, Michael K. Budinski, Craig S. Gittleman, *Characterizing the fracture resistance of proton exchange membranes.* Journal of Power Sources, 2008. **185**(1): p. 374-380.
36. Dillard, D.A., Li, Y., Grohs, J. R., Case, S. W., Ellis, M. W., Lai, Y., Budinski, M., Gittleman, C., *On the Use of Pressure-Loaded Blister Tests to Characterize the Strength and Durability of Proton Exchange Membranes.* Journal of Fuel Cell Science and Technology, 2009. **6**(3): p. 031014-1 - 031014-8.
37. Gittleman, C.S., Lai, Y. H., and Miller, D. P. *Durability of Perfluorosulfonic Acid Membranes for PEM Fuel Cells*. in *Extended Abstract in the AIChE 2005 Annual Meeting*. 2005. Cincinnati, OH.

38. Grohs, J.R., *Analysis and modeling of the mechanical durability of proton exchange membranes using pressure-loaded blister tests*, in *Engineering Science and Mechanics*. 2009, Virginia Polytechnic Institute and State University.
39. Jacob R. Grohs, Y.L., David A. Dillard, Scott W. Case, Michael W. Ellis, Yeh-Hung Lai, Craig S. Gittleman, *Evaluating the time and temperature dependent biaxial strength of Gore-Select® series 57 proton exchange membrane using a pressure loaded blister test.* Journal of Power Sources, 2009. **195**(2): p. 527-531.
40. Lai, Y., Mittelsteadt, C. K., Gittleman, C. S., and Dillard, D. A. *Viscoelastic Stress Model and Mechanical Characterization of Perfluorosulfonic Acid (PFSA) Polymer Electrolyte Membranes*. in *Proceedings of the Third International Conference on Fuel Cell Science, Engineering and Technology*. 2005. Ypsilanti, Michigan.
41. Mathias, M.F., Makharia, R., Gasteiger, H. A., Conley, J. J., Fuller, T. J., Gittleman, C. J., Kocha, S. S., Miller, D. P., Mittelsteadt, C. K., Xie, T., Van, S. G., and Yu, P. T., *Fuel Cell Cars In Every Garage.* Electrochem. Soc. Interf., 2005. **14**: p. 24-35.
42. Michael Pestrak, Y.L., Scott W. Case, David A. Dillard, Michael W. Ellis, Yeh-Hung Lai, Craig S. Gittleman, *The Effect of Mechanical Fatigue on the Lifetimes of Membrane Electrode Assemblies.* Journal of Fuel Cell Science and Technology, 2010. **7**(4): p. 041009-1 - 041009-10.
43. Yeh-Hung Lai, C.K.M., Craig S. Gittleman, David A. Dillard, *Viscoelastic Stress Analysis of Constrained Proton Exchange Membranes Under Humidity Cycling.* Journal of Fuel Cell Science and Technology, 2009. **6**(2): p. 021002-1 - 021002-13.
44. Yeh-Hung Lai, D.A.D., ed. *Mechanical Durability Characterization and Modeling of Ionomeric Membranes*. Handbook of Fuel Cells Volume 5: Advances in Electrocatalysis, Materials, Diagnostics and Durability, ed. H.Y. Wolf Vielstich, Hubert A. Gasteiger. 2009, John Wiley & Sons, Ltd.: Chichester, England.
45. Yongqiang Li, D.A.D., Scott W. Case, Michael W. Ellis, Yeh-Hung Lai, Craig S. Gittleman, Daniel P. Miller, *Fatigue and creep to leak tests of proton exchange membranes using pressure-loaded blisters.* Journal of Power Sources, 2009. **194**(2): p. 873-879.